UNIVERSITAT POLITÈCNICA DE CATALUNYA
BARCELONATECH
Escola Superior d'Enginyeries Industrial,
Aeroespacial i Audiovisual de Terrassa

BACHELOR'S DEGREE THESIS

Study on the Hydrofoil Application on Amphibious Aircrafts

Document:

Report

Author:

Iban Amauri Agirre Mosquera

Director:

Josep Ramón Martínez Piñol

Degree:

Bachelor's Degree in Aerospace Vehicles Engineering

Call:

Spring, 2022

Etxekoei, ibilbide honetan sostengu, motibazio eta kabi izateagatik. Kuadrillari, berotasuzen eta gogoz jastozeagatik nire absentzian. Carrer Mallorca 304-koei, aurtengo aurkikuntza izan zaretelako.

Als meus amics Pol,Dani i Andrés per acompanyar-me en aquesta aventura durant cinc anys. A la persona més important d'aquest últim any, Patricia, per aguantar-me a la frustració i tensió del treball, valorar-me i escoltar-me les xapades de friki.

Declaration of Honor

I declare that

- The work in this Bachelor Thesis is completely my work,
- No part of this Bachelor Thesis is taken from other people's work without giving them credit,
- All the references have been cited,

I understand that an infringement of this declaration leaves me subject to the foreseen disciplinary actions by the "Universitat Politècnica de Catalunya-BarcelonaTECH".

Iban Amauri Agirre Mosquera		22/06/2022
Student's Name	Signature	Date

Project title: "Study on the Hydrofoil Application on Amphibious Aircrafts"

Abstract

This Bachelor's thesis proposes a preliminary study on the use of hydrofoils on amphibian aircraft. It contains a summary on seaplane and hydrofoil technology, followed by theoretical introduction in fluid dynamics and the mathematics applied for the study.

At the beginning, the no-hydrofoil aircraft configuration is developed, using the theoretical background and XFOIL for the airfoil, to obtain its performance as a base for the hydrofoil study. The study progresses with the geometric configuration of the hydrofoil based on the researched theoretical background. The validation of this calculation is made with the OpenFOAM software based on a 2D flow simulation. The optimization of the foils are made by trial and error in the CFD.

Finally, the new hydrofoil platform is designed and later on its performance is compared to the initial configuration to validate the usefulness of the modification.

The author of this study intends to improve the TO performance of amphibian aircraft in order to bring up to date their fuel efficiency, as well as to assist amphibian plane electrification.

Resumen

El trabajo propuesto para este ”Trabajo de fin de grado” es el estudio preliminar en hydrofoils para aviones anfibios. El estudio contiene un resumen en la tecnología de hydroaviones y en hydrofoils, seguido por una introducción al marco teórico de la dinámica de fluidos y su aplicación matemática.

Al principio, se desarrollará la configuración sin hydrofoil del avión, basado en los conocimientos teóricos y en XFOIL para los valores del airfoil, para obtener su actuación base en el estudio. Se progresará con la configuración geométrica del hydrofoil basado en la teoría buscada sobre este tema. La validación de esta configuración se hará mediante el software de simulación de CFD OpenFOAM y en el marco de un flujo 2D. La optimización de dicho perfil se hará mediante CFD también.

Para terminar, la plataforma del nuevo hydrofoil será diseñado y su actuación se comparará con la obtenida inicialmente. De esta forma se validará la utilidad de esta modificación.

El autor de este estudio intenta optimizar el despegue de aviones anfibios para actualizar la eficiencia del gasto de combustible, a la par que apoyar la electrificación de aeronaves.

Contents

List of Tables

List of Figures

Glossary

AC	Aerodynamic Center
ADC	Aircraft Developing Cost
AoA	Angle of Attack
AR	Aspect Ratio
CFD	Computational Fluid Dynamics
CG	Center of Gravity
DNS	Direct Numerical Simulation
EBITDA	Earnings Before Interest Taxes Depreciation and Amortization
GA	General Aviation
IRR	Internal Rate of Return
J3T	Johnson's Three Terms
J5T	Johnson's Five Terms
LES	Large Eddy Simulation
MAC	Mean Aerodynamic Center
MTOW	Maximum Take-off Weight
NACA	National Advisory Committee for Aeronautics
NPV	Net Present Value
RANS	Reynolds Averaged Navier-Stokes
SC	Super Cavitating
STO	Short Take-off
STOL	Short Take-off and Landing
TC	Type Certficate
TE	Trailing Edge
TO	Take-off
2D	2 Dimension
3D	3 Dimension

List of Symbols

B_f	Maximum Hull Beam
b	Wingspan
c	Chord
C_d	2D Drag Coefficient
C_{d_h}	2D Hydrofoil Drag Coefficient
C_{d_0}	Zero Lift Drag Coefficient
C_D	3D Drag Coefficient
C_{D_i}	Induced Drag Coefficient
$C_{D_{i_h}}$	Hydrofoil Induced Drag Coefficient
C_{D_h}	3D Hydrofoil Drag Coefficient
$C_{D_{0_h}}$	3D Hydrofoil Zero Lift Drag Coefficient
C_l	2D Lift Coefficient
$C_{l,d}$	Design Lift Coefficient
C_{l_h}	2D Hydrofoil Lift Coefficient
C_L	3D Lift Coefficient
C_{L_h}	3D Hydrofoil Lift Coefficient
C_{l_α}	2D Lift Coefficient Variation
C_{L_α}	3D Lift Coefficient Variation
C_p	Pressure Coefficient
$C_{p_{min}}$	Pressure Coefficient
C_R	Hull Resistance Coefficient
c_r	Root Chord
c_t	Tip Chord
C_U	Velocity Coefficient
C_Δ	Load Coefficient
C_{Δ_0}	Gross Load Coefficient
$C_{m_{ac}}$	2D Momentum at AC Coefficient
$C_{M_{ac}}$	3D Momentum at AC Coefficient
D	Drag Force
D_h	Hydrofoil Drag Force
D_i	Induced Drag
e	Oswald's Efficiency Number
g	Gravitational acceleration
L	Lift Force
L_h	Hydrofoil Lift Force
M	Momentum
p	Pressure at a Position
p_v	Vapour Pressure
p_∞	Freestream Pressure

q_∞	Freestream Dynamic Pressure
R	Hullf Resistance
Re	Reynolds number
S	Surface
S_h	Hydrofoil Surface
T	Thrust
T_{static}	Static Thrust
U	Velocity
U_{MAX}	Max. Velocity
V	Volume
W	Weight
x	Abscissa Coordinates
y	Ordinate Coordinates
α	Angle of Attack
α_0	Zero Lift Angle of Attack
α_i	Induced Angle of Attack
Δ	Weight Load
λ	Taper Ratio
ν	Kinematic Viscosity
ρ_w	Water Density
ρ	Air Density
σ	Cavitation Number
θ	Angular Foil Position

1 Introduction

1.1 Aim of the Project

This project aims to study the feasibility of hydrofoils on amphibious aircraft in order to reduce TO distances. The research implies designing the hydrodynamic lifting surfaces, as well as studying their general geometry and location.

1.2 Justification

Amphibian aircraft are a niche sector of the aeronautical industry, where many companies compete in the light aircraft market, such as Lisa Akoya [11], Icon A5 [9] and Seamax M-22 [17]. However, the development is limited on planes with a MTOW heavier than 5000 kg. For instance, the CL-215/415, Canadair's amphibian aircraft developed in the 1960s, has received two updates. These where narrowed down to the improvement of the avionics, electric system, fuel system, MTOW and flight safety [3].

Figure 1.1: Lisa's light sports plane with its hydrofoil devices.

On the other hand, advanced innovations occur in the military, where fuel efficiency is not a concern. In the case of the US-2, the STOL is obtained by blowing air to the extrados via a turboshaft compressor [19]. This kind of development can not be transferred to the GA industry as it is not cost effective, nor environmentally friendly.

Nonetheless, since the previous decade, the sailboat industry has been developing the use of hydrofoils. This devices lifts the totality of the hull from the water, drastically reducing the generated drag and obtaining higher speeds. For example, the top speed record of the AC75 sailboat is 53.31Kn (98.73kph) in the 2021 Prada Cup semifinals [7].

Figure 1.2: Luna Rossa's AC75 sailing over the sea in one of the Prada Cup Regatta.

The project intends to provide a preliminary study on the use of hydrofoils on an over 5000kg amphibian aircraft in order to improve the take-off performance, therefore improving fuel efficiency. Moreover, the subject of study itself is of great interest for the student. Therefore, it will be a great opportunity to apply the acquired knowledge during the previous years.

1.3 Scope

In this project the developed areas will be the following ones:

- Theoretical introduction to hydrodynamics.
- Hydrofoils's background study.
- Hydrofoils and amphibian aircraft state of the art review.
- Aircraft selection based on the amount of data rather than performance.
  - Modifications would not be studied, they must be obtained from databases.
- Selection of the lifting platform type, where advantages and disadvantages would be considered.
- Definition of the lifting surface dimension and geometry based on calculations and theoretical background.
- 2D CFD testing of the hydrofoil (Open FOAM).

- A stability study would not be performed.
  - The TO performance would be considered in level flight and calm water.
- Study on the economic feasibility of the project.
- Calculate the environmental impact of the project.

1.4 Requirements

- The aircraft must have an MTOW higher than 5000kg.
- TO distance must be improved, this means that the overall drag must be lower than in the initial configuration. The added lifting elements must not generate enough aerodynamic drag to endanger the take-off once on air.
- The fuselage can be partially lifted by the hydrowing during the take-off run.

2 State of the Art

Although Lisa Akoya is the sole amphibian aircraft with hydrofoils in production, the US NAVY did research the application of aquatic lifting devices in the 70s. On this study, the team performed calculations around various hydrofoils performance. The project also included trials which used experimental designs on the Grumman Goose JRF-5, one with water ski configuration and another one with hydrofoils (figure 2.1 and 2.2) [22]. As J. Frey stated on a interview [13], the government discontinued the investigation as the military air force shifted to the more versatile helicopters and aircraft carriers.

Figure 2.1: JRF5 waterski config.

Figure 2.2: JRF5 hyrdrofoil config.

2.1 Selected Aircraft

Being the MTOW one of the limiting factors of the requirements, the aircrafts with the greatest amount of data were the Canadair CL-415, Viking DHC-6 and Shinmaywa US-2. A previous report used a modified design of a DHC-6 with a NACA TN2481 [20] planning hull in order to study a hydrofoil on a boat-plane [18]. Therefore, using the same design could be useful to compare results, as well as applying its suggestions.

The Viking DHC-6 is a twin turboprop and high winged aircraft designed by de Haviland Canada in 1965 and its production lasted until 1988, manufacturing 844 aircraft. In 2005 Viking purchased de Havilland Canada's TCs of all the out of production planes, bringing back to production de DHC-6 400 in 2007 [23].

This plane can operate in highly diverse climate, from North Africa deserts to the South Pole (the only aircraft capable of performing emergency evacuations of critical patients on

$-60°C$). Moreover, it offers the ability to attach skis for the snow and floats for water operations. However, the water TO distance increases in comparison with the land tricycle configuration. On land, it is able to perform a STO in 366 *m*, while the float-plane configuration takes off in 599 *m* (both climbing to 50 *ft*) [23].

The NACA TN2481 is a low-drag, planning-tail hull designed in 1950s and is based on previously tested hull models. Its main objective is to reduce TO and flight drag. The Technical Note shows the parameters of the hull design, as well as non-dimensional results and plots of the tests. All of these data eases the development of this study.

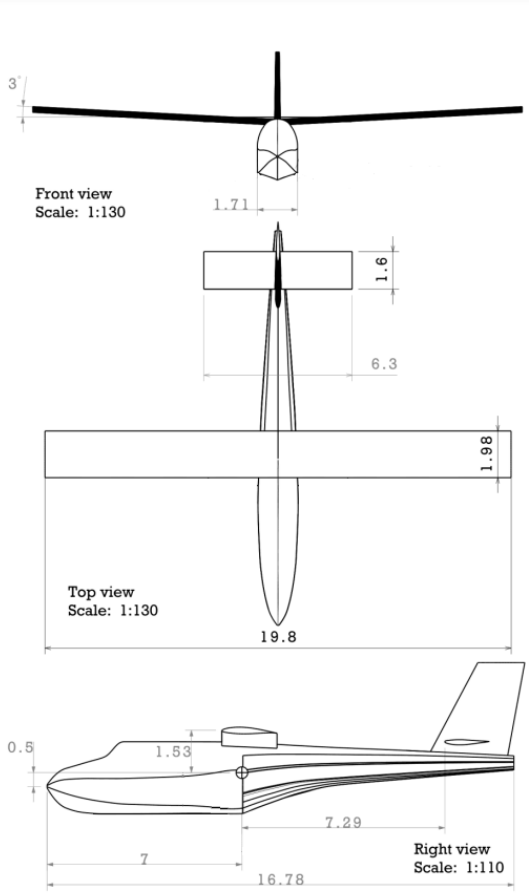

Figure 2.3: DHC-6 with NACA TN2481 flying hull blueprint by Arjit Seth and Rhea P. Liem [18].

Parameters	Value
MTOW	5670 kg
PT6A-34	583.883 kW
Wing	Top wing
Wingspan	19.8 m
Wing chord	1.98 m
H. estabilizer	6.3 m
H. chord	1.6 m
AR	10
Dihedral	3°
Hull	NACA Planning Hull
Hull Beam	1.71 m

Table 2.1: Selected Aircraft Parameters.

2.2 Hydrofoil

A hydrofoil is a water based airfoil. Which, at the same Reynold's number, the same foil creates equal moments and forces in the air as in the water. As water density is higher, these type of foils are limited to be used at low speeds in order to maintain the flow fully attached (subcavitating).

Higher speed regimes imply that flow separation occurs, substantially reducing the efficiency. As water vehicles, and especially amphibian aircraft, operate at higher speeds, where cavitation is unavoidable, a new hydrofoil design is required. The new foil is named supercavitating hydrofoil, its characteristics are: sharp leading edge of 6°, shaped as a wedge and with blunt trailing edges.

2.2.1 Cavitation

A foil moving through the water producing lift generates an increase in pressure on the intrados and a pressure decrease on the extrados. This pressure differential depends on the hydrofoil shape, velocity, AoA and operation depth (ambient pressure). This means that, for a given hydrofoil, as we increase the velocity and AoA and decrease in depth, the pressure in the intrados will decrease until reaching the water vapour pressure. At this moment the water will start boiling (cavitating), similar to the flow separation on an airfoil and the critical Mach effects on aerodynamics.

The aerodynamic pressure coefficient is also useful in the hydrodynamics as it is independent of flow velocity. At flow separation regime the C_p reaches its minimum value indicating cavitation.

$$C_p = \frac{p - p_\infty}{q_\infty} \rightarrow C_{p_{min}} = \frac{p_v - p_\infty}{q_\infty} \tag{2.1}$$

In hydrodynamics, the negative of the pressure coefficient is defined as the cavitation number.

$$\sigma = \frac{p_\infty - p_v}{q_\infty} \tag{2.2}$$

As the value of σ gets lower, the cavitation advances over the extrados. When the cavitation is near the trailing edge, the re-entrant jet and the eddies still exist closing the cavity, where buffeting and foil vibration become an issue. However, if σ keeps getting lower, the cavity lengthens to a point where the re-entrant jet is dissipated. This flow is known as supercavitating and the cavity length reaches over two times the chord.

2.2.2 Ventilation

Ventilation is known as the phenomenon where the cavitation is pressurized via natural methods or forced engineered methods.

The natural ventilation is a phenomenon where atmospheric air passes into the low pressure zone of the hydrofoil, usually through the surface piercing strut or the blunt trailing edge of the foil. In order for natural ventilation to occur, the cavitation must be established and completely developed to its final state.

In partial cavitation conditions, ventilation can result in the loss of up to 76% of the lift, as a consequence the supported vehicle will experience a fall. Regrettably, the behaviour of natural ventilation can not be predicted analytically neither from model tests.

On the other hand, hydrofoils operating at supercavitating conditions will experience little effect on the forces. The main difference will be experienced on the pressure, therefore when calculating the σ, p_v must be changed for p_c (air pressure of the cavity).

Forced ventilation can be obtained by blowing pressurized air to the section where cavitation is needed ,but no natural ventilation is contemplated. However, this forced development of cavitation will create changes on the lift and drag.

2.2.3 Selected Hydrofoils

For this study the selected type of hydrofoil is a SC hydrofoil as the aircraft's TO speed is considered to be relatively high and a fully developed cavitation is expected.

As Stefano Brizzolara states [2], the design method used nowadays is based on using CFD simulations to complement the classical potential flow solutions. The idea is to define the intrados with potential flow solutions, as the lift depends on its form. Afterwards, a series of simulations will be run to define the extrados by trial and error.

Brizzolara presents three methods in his report, Tulin-Burkhart's (1955) linear theory and the Johnson's (1961) three and five terms profiles. However, it is shown that Johnson's profiles both obtain "new shapes with higher efficiencies" [2]. Therefore, the used solutions will be the latter two.

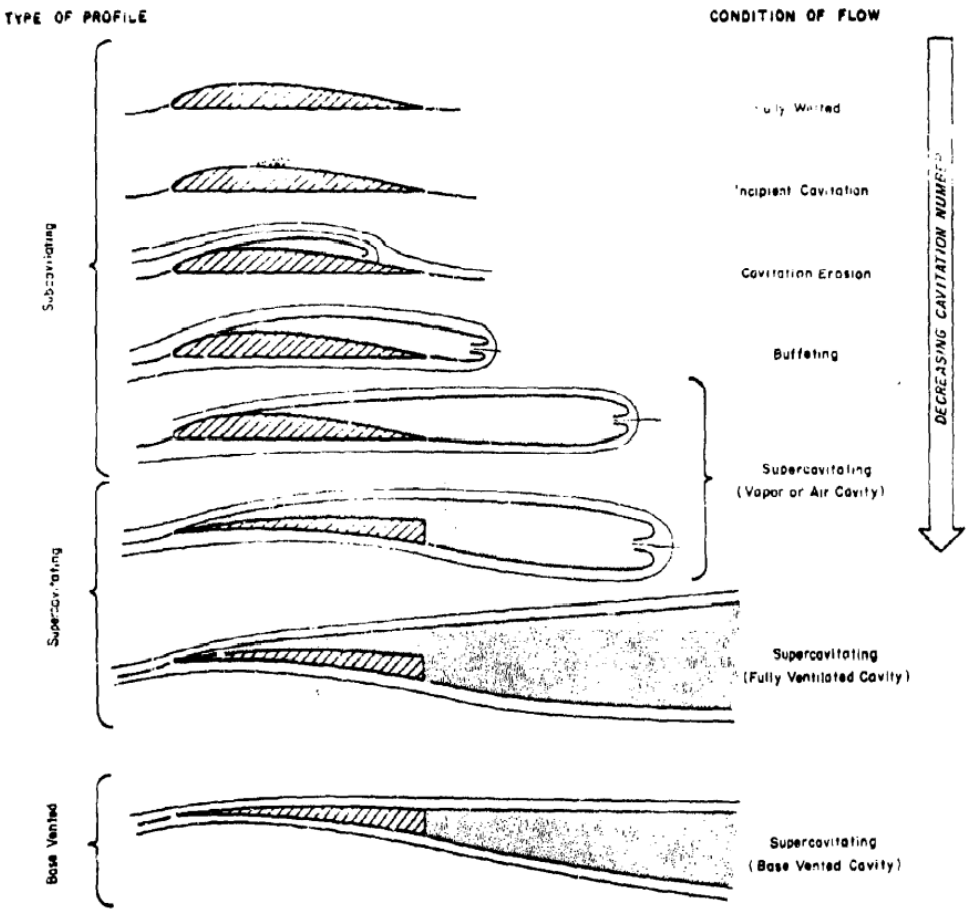

Figure 2.4: Hydrofoil geometry in function of cavitation number.

2.3 Hydrowing

It is expected that the dynamics of a subaquatic wing follows the same principles of a traditional wing. Hence, a hydrowing will generate lift, drag and a momentum in the MAC. It should be pointed out that during the TO roll longitudinal control will be available from the empennage. However, as the development of hydrofoils for amphibian aircraft has not matured enough, no standard configuration is established yet.

In the study performed by the US NAVY two wing configuration were tested: the single hydrofoil system and the Grunberg system. In the first case, the wing is located a bit forward from the aircrafts CG and the longitudinal stability is provided solely by the horizontal stabi-

lizer. In the second system a main lifting surface (continuous or split) is located after the CG and a pair of water skis are located forwards in order to provide stability and extra lift force. Finally, the Lisa Akoya uses a split Tietjens system, where the configuration resembles one of a traditional plane (main forward surface stabilized by an smaller surface). Figure 2.5 shows the wing configuration discussed by the US NAVY [22].

Apart from the platform system, the attachment has many variants. However, being a preliminary design, this part will not be discussed and a monofoil system is selected (no interactions between the strut and the wing will be studied). Said system does not generate interferences between wings as a ladder system would do, nor require a more complex mechanism as a hoop wing.

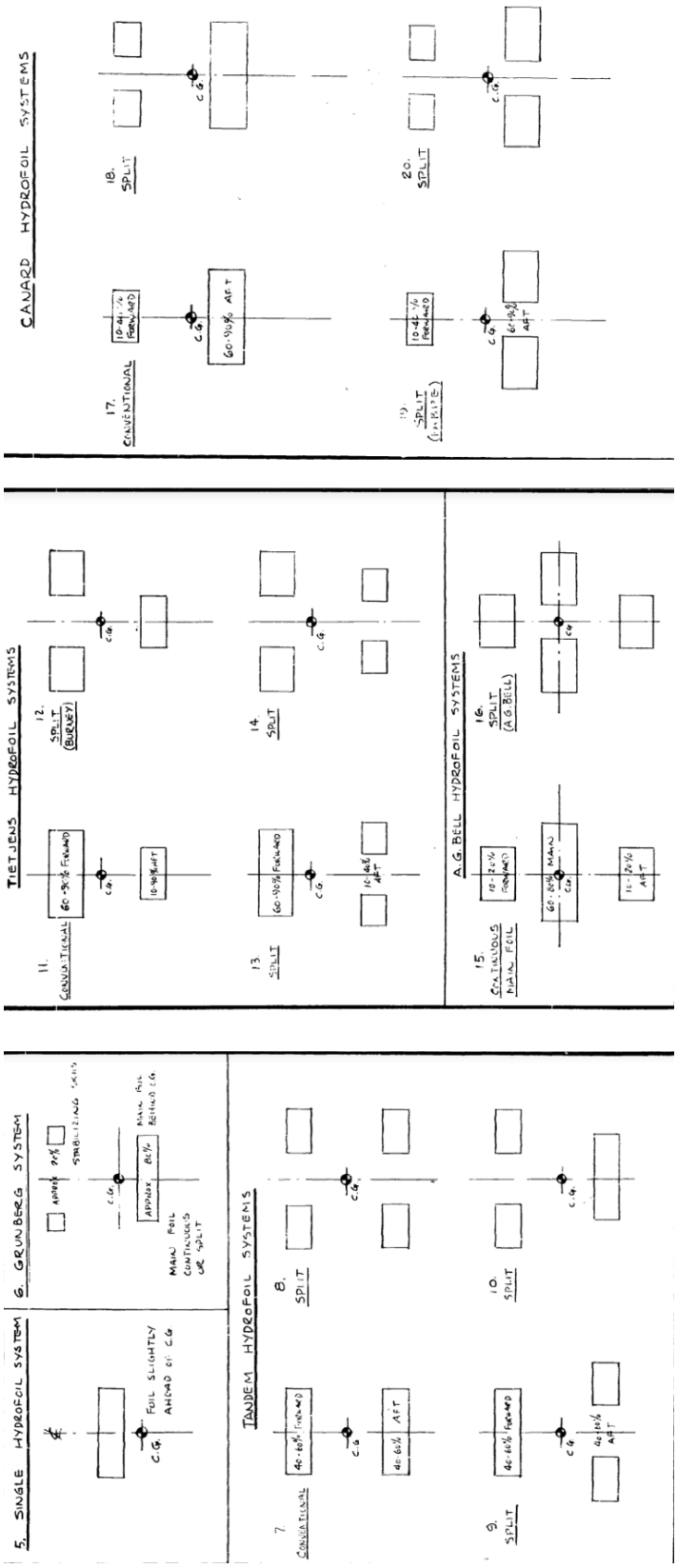

Figure 2.5: Hydrofoil attachment systems.

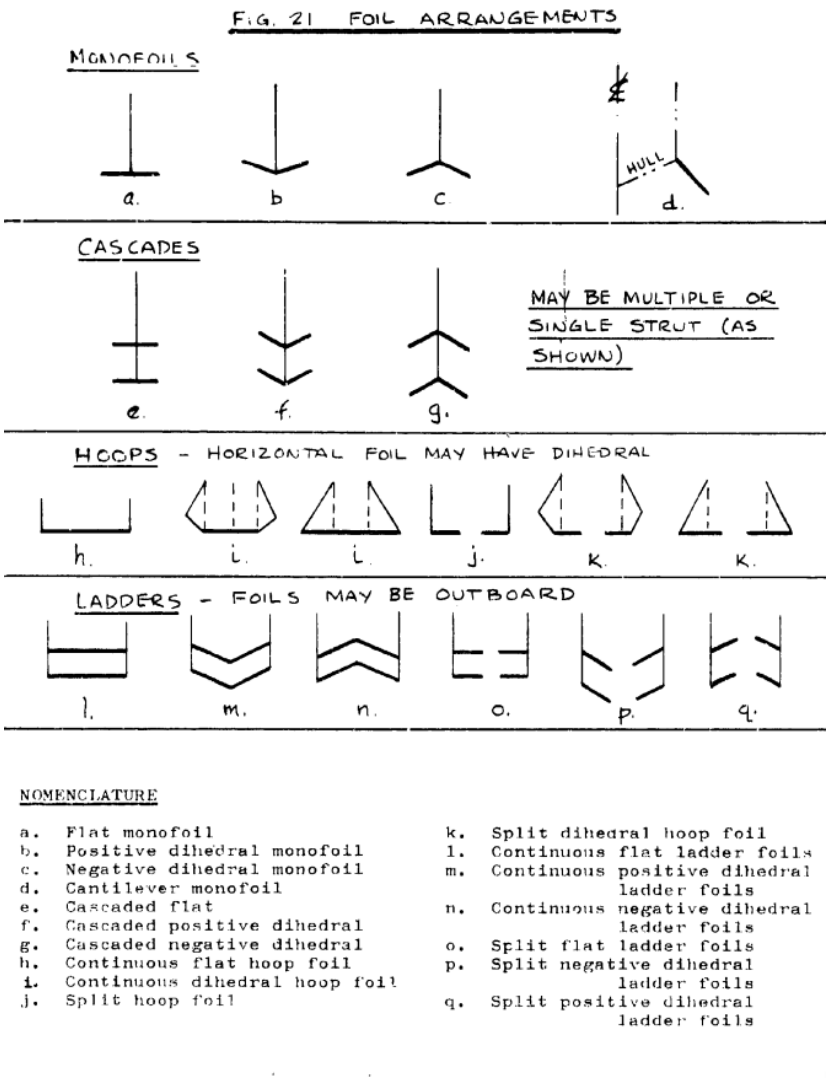

Figure 2.6: Hydrofoil attachment systems from the US NAVY [13].

2.4 Theoretical Background

2.4.1 Flying Hull

The used flying hull from the Technical Note TN2481 [20] normalizes the forces and moments experienced by the aircraft. For this study, the relevant forces are the load and the resistance, the latter being dependent on speed.

The velocity coefficient is defined as a variation of the Froude number, where B_f is the maximum beam of the hull:

$$C_V = \frac{U}{\sqrt{gB_f}} \tag{2.3}$$

The resistance coefficient is the empirical data obtained in this note and is expressed as:

$$C_R = \frac{R}{\rho_w g B_f^3} \tag{2.4}$$

The load factor is:

$$C_\Delta = \frac{\Delta}{\rho_w g B_f^3}, \ \Delta = W - \sum_i L_i \tag{2.5}$$

Arjit and Rhea explain the maximum submerged volume is known as the gross load coefficient:

$$C_{\Delta_0} = \frac{W}{\rho_w g B_f^3} \tag{2.6}$$

2.4.2 Fluid Dynamics

2.4.2.1 Principles of an Airfoil

It is important for this study to introduce the theory behind an airfoil in order to design and size the hydrofoil due to the similarity between them.

An airfoil is an aerodynamic device designed to create lift. When submerged into a stream, the fluid diverts due to the Coanda effect and follows the perimeter of the profile. At the trailing edge of the foil it keeps the direction tangent to the foil, where the merge of flows has a downwards direction. This results on a reaction of equal magnitude experienced by the airfoil, as Newton's third law indicates. On the other hand, this flow division creates a pressure differential too, the extrados experiences a pressure decrease, while the intrados experiences a pressure increase. As a consequence, the resultant force on the airfoil is diagonally upwards (lift and drag).

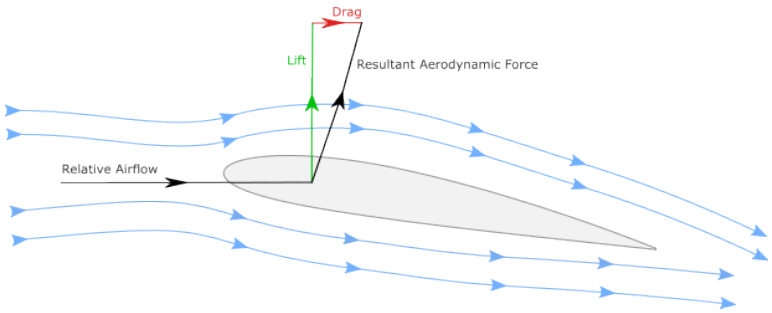

Figure 2.7: Flow around an airfoil and the experienced aerodynamic force.

The concept of boundary layer must be introduced. All fluid particles have the tendency to maintain the velocity of the adjacent particle. Therefore, when a fluid is in contact with a solid surface, whose velocity is zero, the fluid particles in direct contact with the surface also have a velocity equal to zero. Thus creating a velocity gradient known as the boundary layer.

The boundary layer can be either laminar or turbulent. A rule of thumb to expect the transition point between laminar and turbulent is by the Reynolds number ($Re < 3x10^6$ *laminar*).

$$Re = \frac{\rho c|U|}{\nu} \tag{2.7}$$

- Laminar boundary layer: the flow throughout the foil maintains a structured form and the height of said layer is smaller than a turbulent one. On the other hand, the velocity profile has a parabolic form. However, obtaining a laminar boundary layer through all the foil is extremely difficult and it is natural experiencing a transition to turbulent flow.
- Turbulent boundary layer: for this case the flow is chaotic and unstructured. This is due to an increase on the kinetic energy. As a result, the layer generates a higher drag force. However this higher energy state helps to maintain the flow attached to the foil.

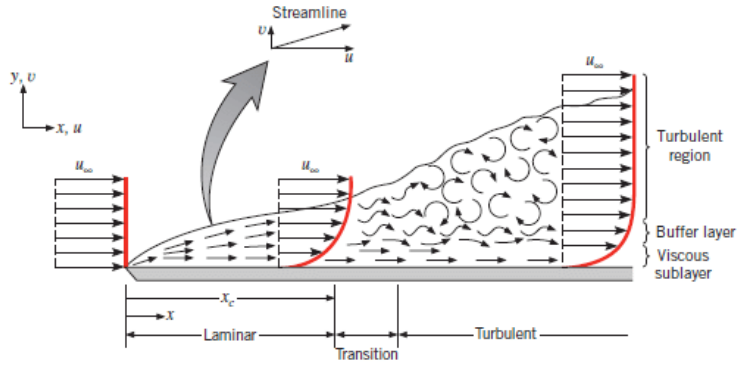

Figure 2.8: Flow transition from laminar to turbulent boundary layer.

The behaviour of a foil can be determined by the coefficients of lift, drag and momentum at the AC . The lift coefficient for a known regime only depends on the AoA and on the linear section. The latter can be expressed by the slope C_{l_α} and the angle variation, where α_0 is the AoA for zero lift. Followed by the linear section the curve reaches its maximum point after which the C_l will keep decreasing. This point is also known as the stall point.

$$C_l = \frac{L}{\frac{1}{2}\rho|U|^2 c}, \; C_l = C_{l_\alpha}(\alpha - \alpha_0) \tag{2.8}$$

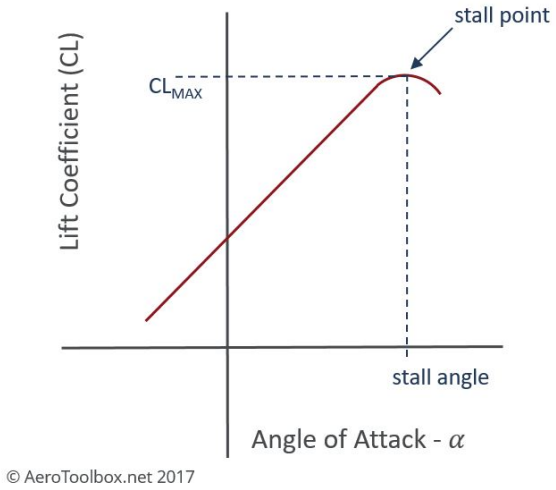

Figure 2.9: C_l vs. α.

In the case of the drag coefficient, its curve can be approximated to a parabola. For the case of the C_d it is dependent on the C_l. The parasite drag coefficient is obtained when the lift is zero and it does not need to be equal to the $C_{d_{min}}$. The parabolic approximation is only accurate for AoA below 5°.

$$C_d = \frac{D}{\frac{1}{2}\rho|U|^2 c} = C_{d_0} + jC_l + kC_l^2 \tag{2.9}$$

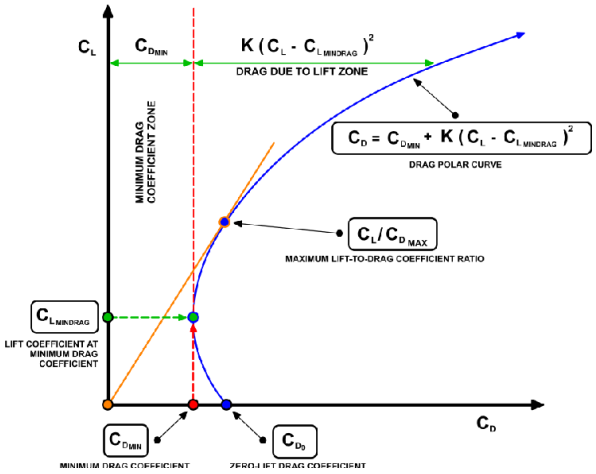

Figure 2.10: C_l vs. C_d.

The momentum of the foil is not in the scope of this project, therefore only the C_m is shown.

$$C_{m_{ac}} = \frac{M}{\frac{1}{2}\rho|U|^2 c^2} \tag{2.10}$$

The two-dimensional coefficients are obtained from an ideally infinite wing, where wing tip eddies are not taken into account. As a result, the three-dimensional lift slope is obtained from Prandtl's elliptical platform theory, completed with Oswald's efficiency number for non elliptical wings [12].

$$C_{L_\alpha} = \frac{C_{l_\alpha}}{1 + \frac{C_{l_\alpha}}{\pi AR}} e \tag{2.11}$$

This way, the 3D lift coefficient is defined as:

$$C_L = \frac{L}{\frac{1}{2}\rho|U|^2 S} \; C_L = C_{L_\alpha}(\alpha - \alpha_0) \tag{2.12}$$

The before mentioned down-wash also affects on the three dimensional drag, generating an induced drag $D_i = L\alpha_i$, being $\alpha_i = \frac{C_L}{\pi AR}$ the induced AoA. The combination of the two expressions results in:

$$D_i = L\frac{C_L}{\pi AR} \rightarrow C_{D_i} = \frac{C_L^2}{\pi AR} \tag{2.13}$$

This expression is useful for an elliptical platform, therefore Oswald's efficiency factor must be taken into account again for the 3D drag coefficient.

$$C_D = \frac{D}{\frac{1}{2}\rho|U|^2 S} \; C_D = C_{D_i} + C_{d0} = \frac{C_L^2}{\pi AR} e + C_{d0} \tag{2.14}$$

As mentioned before the stability of the aircraft is not a concern, thus the definition of the 3D moment coefficient is limited to the adimensionalization.

$$C_{M_{ac}} = \frac{M}{\frac{1}{2}\rho|U|^2 Sc} \tag{2.15}$$

2.4.2.2 Governing Equations of the Flow

In this study, both airfoil and hydrofoil 2D flow simulations will be carried out to obtain the moments and forces on the foil. Both cases share the same hypotheses, as water and air are Newtonian fluids on a turbulent flow. Although air can be compressible, at a flow regime below $0.3 \cdot M$ it behaves as incompressible.

Hypotheses:

- Incompressible flow
- Turbulent flow
- Newtonian flow
- Bi-dimensional flow
- Sea level conditions

Due to the nature of the problem, no easy analytical solution is possible. But, is important to keep in mind the main equations which govern the flow. These Being the continuity equation, the momentum equation and the equations related to the turbulent flow.

The continuity equation indicates that no matter can be created or destroyed, therefore the matter in our volume of control must be constant. Its mathematical definition:

$$\frac{d}{dt}\int_V \rho\, dV = -\int_S \rho\vec{u}\cdot\vec{n}\, dS \tag{2.16}$$

The differential form of the continuity equation can be obtained by Gauss's Divergence Theorem:

$$\frac{\delta\rho}{\delta t} + \nabla\cdot(\rho\vec{u}) = 0 \tag{2.17}$$

The extended expression being:

$$\frac{\delta\rho}{\delta t} + \frac{\delta(\rho u_x)}{\delta x} + \frac{\delta(\rho u_y)}{\delta y} + \frac{\delta(\rho u_z)}{\delta z} = 0 \tag{2.18}$$

As mentioned before the defined flow is incompressible, meaning that there is not density differential:

$$\nabla\cdot(\rho\vec{u}) = 0 \tag{2.19}$$

$$\frac{\delta u_x}{\delta x} + \frac{\delta u_y}{\delta y} + \frac{\delta u_z}{\delta z} = 0 \tag{2.20}$$

The momentum equation comes from Newton's second motion law: the resultant force is equal to the product of the mass and acceleration of the object. For a static control volume:

$$\frac{\delta}{\delta t}\int_V \vec{u}\,\rho\, dV + \int_S \vec{u}\,\rho\vec{u}\cdot\vec{n}\, ds = \int_S \overrightarrow{f_{\vec{n}}}\, dS + \int_V \vec{f_b}\, dV \tag{2.21}$$

In this equation the left hand side represents the rate of change of the linear momentum inside the volume and its flux through the surface. For the right side, the terms represent

surface and volume forces. The latter is the sum of gravitational forces, Coriolis effect, fictitious and electromagnetic forces. In the case of the surface forces, the sum is between the pressure and viscous forces.

As for the continuity equation, the differential form is obtained by applying the Gauss's Divergence Theorem.

$$\frac{\delta(\rho\vec{u})}{\delta t} + \nabla\cdot(\rho\vec{u}\,\vec{u}) = -\nabla p + \nabla\cdot\vec{\tau} + \sum F^b \tag{2.22}$$

The extended definition being:

$$\frac{\delta(\rho u_x)}{\delta t} + \frac{\delta(\rho u_x u_x)}{\delta x} + \frac{\delta(\rho u_y u_x)}{\delta y} + \frac{\delta(\rho u_z u_x)}{\delta z} = -\frac{\delta p}{\delta x} + \frac{\delta \tau_{xx}}{\delta x} + \frac{\delta \tau_{yx}}{\delta y} + \frac{\delta \tau_{zx}}{\delta z} + \sum F_x^b$$

$$\frac{\delta(\rho u_y)}{\delta t} + \frac{\delta(\rho u_x u_y)}{\delta x} + \frac{\delta(\rho u_y u_y)}{\delta y} + \frac{\delta(\rho u_z u_y)}{\delta z} = -\frac{\delta p}{\delta y} + \frac{\delta \tau_{xy}}{\delta x} + \frac{\delta \tau_{yy}}{\delta y} + \frac{\delta \tau_{zy}}{\delta z} + \sum F_y^b$$

$$\frac{\delta(\rho u_z)}{\delta t} + \frac{\delta(\rho u_x u_z)}{\delta x} + \frac{\delta(\rho u_y u_z)}{\delta y} + \frac{\delta(\rho u_z u_z)}{\delta z} = -\frac{\delta p}{\delta z} + \frac{\delta \tau_{xz}}{\delta x} + \frac{\delta \tau_{yz}}{\delta y} + \frac{\delta \tau_{zz}}{\delta z} + \sum F_z^b$$

Where τ is defined by Stoke's law on Newtonian fluids:

$$\vec{\tau} = \mu(\nabla\vec{u} + (\nabla\vec{u})^T) - \frac{2}{3}\mu(\nabla\cdot\vec{u})\vec{\delta} \tag{2.23}$$

Being an incompressible flow, $\nabla\cdot\vec{u} = 0$, the combination of (2.22) and (2.23):

$$\frac{\delta(\rho\vec{u})}{\delta t} + \nabla\cdot(\rho\vec{u}\,\vec{u}) = -\nabla p + \nabla\cdot(\nabla\vec{u} + (\nabla\vec{u})^T) + \sum F^b \tag{2.24}$$

2.4.2.3 Turbulence Models

Previously it is mentioned the chaotic nature of a turbulent flow. However, it still complies with the Navier-Stokes equation. The problem with this type of flows is its non linearity, as it is constantly interacting between various flow structures, different length eddies. Therefore, no analytic neither numerical solution is attainable.

On the other hand, a total computational solution is not possible for the same reason: the multi scale flow structures. Turbulence models have been created to emulate the behaviour of said structures up to a defined threshold. The three main solvers are DNS, LES and RANS [6].

- **DNS**: Direct Numerical Simulation operates by solving Navier-Stokes without a model. This means that the scales that influence dissipation are resolved. The relationship between the characteristic length and the smallest length scale for dissipation is rep-

resented by:

$$\frac{L}{\eta} = \Theta(Re^{\frac{3}{4}}) \tag{2.25}$$

This relationship indicates the number of grid points necessary to solve the given flow. Although local results of DNS make no sense due to the chaotic behaviour of the flow, it can resolve the behaviour of a turbulent flow over its characteristic time by taking those averages.

- **LES**: The Large Eddy Simulation is based on the principle that small eddies are isotropic, therefore they dissipate most of the heat and are not dependent of the flow field. This way, it resolves the larger eddies and models the ones expected to be isotropic.To obtain this large eddy solution a field containing only them is required. This is obtained by filtering based on the length scale. Afterwards, vortices under a certain threshold are modelled instead, sub-grid scale vortices. All this process is highly demanding for the computer and is limited as a research tool rather than an engineering one.

- **RANS**: Reynolds Averaged Navier-Stokes is obtained by averaging the smaller scale fluctuations and modelling the non linear behaviour of the flow. The limiting factor is that the flow field must be a steady state and uniform. Therefore RANS is limited to engineering problems, therefore this model is the one used for the study.

2.4.2.4 RANS Equations

For the incompressible flow stated for the study, the RANS equations are defined this way, beginning with the Reynolds averaging laws:

$$\vec{u} = \overline{\vec{u}} + \vec{u'} \tag{2.26}$$

$$\overline{\vec{u}} = \overline{u_x}\,\vec{i} + \overline{u_y}\,\vec{j} + \overline{u_z}\,\vec{k}$$

$$\vec{u'} = u'_x\,\vec{i} + u'_y\,\vec{j} + u'_z\,\vec{k}$$

$$p = \overline{p} + p' \tag{2.27}$$

This equations are applied to the previously discussed flow conservation equations (2.19) and (2.24):

$$\nabla \cdot (\rho \overline{\vec{u}}) = 0 \tag{2.28}$$

$$\frac{\delta(\rho \overline{\vec{u}})}{\delta t} + \nabla \cdot (\rho \overline{\vec{u}}\,\overline{\vec{u}}) = -\nabla \overline{p} + (\nabla \cdot (\overline{\tau} - \rho \overline{\vec{u}}\,\overline{\vec{u}})) + \overline{\sum F^b} \tag{2.29}$$

$\rho\overrightarrow{u'u'}$ is known as the Reynolds stress tensor $\overrightarrow{\tau}^R$, which is a new unknown variable. Being a turbulent flow, the non linearity would continue creating more unknown variables, therefore, as Carlos Cuesta states [6], a turbulence model is required.

Boussinesq hypothesis is a common model for the Reynolds stress tensor. The basis of the hypothesis is that the eddies turbulent motion is supposed to be caused by the random motion of the particles. This is related to the mean velocity gradient and eddies diffusion, creating a similar expression to the Stoke's one for Newtonian fluids.

$$\overrightarrow{\tau}^R = \mu_T(\nabla\overrightarrow{u} + (\nabla\overrightarrow{u})^T) - \frac{2}{3}\rho\overrightarrow{k}\overrightarrow{\delta} \tag{2.30}$$

$$k = \frac{1}{2}(\overrightarrow{u'}\cdot\overrightarrow{u'})$$

On this equation μ_T is the turbulent eddy viscosity (the kinematic eddy viscosity $\nu_T = \mu_T/\rho$) and $\overrightarrow{k}$ is the turbulent kinetic energy.

2.4.3 Johnson's three and five term profiles

Johnson's approach to potential flow solving is based on Tulin-Burkart's technique. This is due to the capability of solving any surface configuration as long as the pressure stays positive at the intrados and the AoA and camber are small. The SC problem is transformed from the complex Z plane to an airfoil problem complex $\bar{Z}$ plane, obtaining the following relationships as Johnson [10] indicates:

$$Z = \sqrt{\bar{Z}} \tag{2.31}$$

$$\frac{d\bar{y}}{d\bar{x}}(\bar{x}) = \frac{dy}{dx}(\bar{x}^2) \tag{2.32}$$

$$\bar{u}(\bar{x}) = u(\bar{x}^2) \tag{2.33}$$

$$C_L = \bar{C}_m = \frac{\pi}{2}\left(A_0 + A_1 + \frac{A_2}{2}\right) \tag{2.34}$$

$$C_D = \frac{1}{8\pi}\bar{C}_L^2 = \frac{\pi}{2}\left(A_0 + \frac{A_1}{2}\right)^2 \tag{2.35}$$

$$C_m = \bar{C}_{m,3} = \frac{\pi}{32}\left(5A_0 + 7A_1 - 7A_2 + 3A_3 - \frac{A_4}{2}\right) \tag{2.36}$$

The airfoil vorticity distribution is expressed by a sine series where the A_n coefficients are the same as the thin-airfoil theory coefficients.

$$\Omega(\theta) = 2V\left(A_0\, cot\,\frac{\theta}{2} + \sum_{n=1}^{\infty} A_n sin\, n\theta\right) \tag{2.37}$$

Glauert's coordinate transformation is used for x along the cord in order to transform into θ, the angular coordinate.

$$\bar{x} = \frac{1}{2}\bar{c}\,(1 - cos\,\theta)\ \ , 0 \leqslant \theta \leqslant \pi \tag{2.38}$$

$$A_0 = \alpha - \frac{1}{\pi}\int_0^{\pi} \frac{d\bar{y}}{d\bar{x}}\, d\theta \tag{2.39}$$

$$A_n = \frac{2}{\pi}\int_0^{\pi} \frac{d\bar{y}}{d\bar{x}}\, cos\, n\theta\, d\theta \tag{2.40}$$

In order to simplify the solving process, A_0 is set $A_0 = 0$. This means that the reference axis is equal to the integral and the AoA is 0. The lift-drag ratio from equations (2.34) and (2.35) lead to:

$$\frac{C_L}{C_D} = \frac{L}{D} = 4(1 - \frac{1}{2}\frac{A_2}{A_1})^2\frac{\pi}{2C_L} \tag{2.41}$$

For a Tulin-Burkart section only two terms of A_n are needed and, as L/D being maximum is intended, Johnson states: $-\frac{A_2}{A_1} = \frac{1}{2}$. Tulin-Burkart's lift-drag ratio is:

$$\frac{L}{D} = \frac{25}{4}\frac{\pi}{2C_L} \tag{2.42}$$

In the case of the three term solution, the used coefficients are up to A_3. As a consequence the lift-drag ratio improves by a 1.44 the Tulin-Burkart's ratio:

$$\frac{L}{D}|_{J3T} = \frac{9\pi}{2C_L} \simeq 1.44\frac{L}{D} \tag{2.43}$$

The lift coefficient is only dependent on the AoA and A_1. In the case of the design lift coefficient, the AoA will be supposed to be 0.

$$C_l = \frac{\pi}{2}(\alpha + \frac{3A_1}{2}) \rightarrow C_{l,d} = \frac{3\pi A_1}{4} \tag{2.44}$$

The Johnson's three term solution defines this intrados shape:

$$\frac{y}{c} = \frac{A_1}{10}\left[5\frac{x}{c} - 20\left(\frac{x}{c}\right)^{\frac{3}{2}} + 80\left(\frac{x}{c}\right)^{2} - 64\left(\frac{x}{c}\right)^{\frac{5}{2}}\right] \tag{2.45}$$

On the other hand, for the five term solution, the used coefficients are increased up to A_5. The lift-drag coefficient improves greatly in comparison to the previous two.

$$\frac{L}{D}|_{J5T} = \frac{50\pi}{9C_L} \simeq 2\frac{L}{D} \tag{2.46}$$

For this case, the C_l definition has a similar form:

$$C_l = \frac{\pi}{2}(\alpha + \frac{5A_1}{3}) \rightarrow C_{l,d} = \frac{5\pi A_1}{6} \tag{2.47}$$

The Johnson's five term solution defines this intrados shape:

$$\frac{y}{c} = \frac{A_1}{315}\left[210\frac{x}{c} - 2,240\left(\frac{x}{c}\right)^{\frac{3}{2}} + 12,600\left(\frac{x}{c}\right)^{2} - 30,912\left(\frac{x}{c}\right)^{\frac{5}{2}} + 35,840\left(\frac{x}{c}\right)^{3} - 15,360\left(\frac{x}{c}\right)^{\frac{7}{2}}\right] \tag{2.48}$$

J5T solution's higher L/D ratio implies a more complex foil geometry. The selection of the foil definition would be a major cost reducing factor. Thus, the simpler J3T geometry has been chosen.

3 Design

After discussing the theoretical and contemporary background, a brief description of the development procedure will be made.

First of all, the forces of the modified DHC-6 must be done. This way, the TO regime is obtained, which is necessary for an initial parametrization of the hydrofoils. Moreover, the basis for the comparison with the new DHC-6 with hydrofoil attachment is obtained.

The parametrization of the hydrofoil is made with the J3T solution and will be simulated via 2D CFD simulation in OpenFOAM. Afterwards, a final hydrofoil selection will be made in order to design the hydrowing and its geometry. Finally, the comparison of the two aircraft models will be made.

3.1 Initial Aircraft Model

For the dynamic solution of the initial aircraft model the following hypothesis are formulated:

- Performance at sea level: $\rho = 1.225\,kg$.
- Constant aircraft attitude: $\alpha = ct$.

The dynamic sketch for the boatplane is showed in Figure 3.1. Here L is the lift force vector, D is the aerodynamic drag, R is the hydrodynamic drag, mg is the weight and T is the total available thrust.

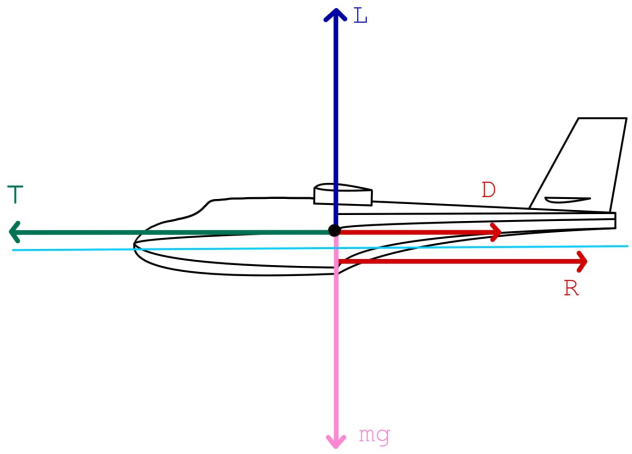

Figure 3.1: DHC-6 dynamic sketch.

In order to occur TO, the lift must be equal to the aircraft's weight. In this case, the weight will be calculated with the MTOW.

$$\vec{L} = \vec{g} \cdot MTOW = 9.81 \cdot 5670 = 55622.7\,N \tag{3.1}$$

The lift is dependent on the speed and the wing's geometry. As a wing does not perform exactly as an ideal airfoil, the wing's C_L varies with its platform geometry:

$$L = C_L \frac{1}{2}\rho U_\infty^2 S = C_{L_\alpha}(\alpha - \alpha_0)\frac{1}{2}\rho U_{inf}^2 S \tag{3.2}$$

Where α is the selected AoA, α_0 is the zero lift AoA, U_∞^2 is the free stream velocity and C_{L_α} is the wing's $\frac{dC_L}{d\alpha}$ on the linear part. The latter is the variable which depends on the platform geometry and is defined by the previously discussed Prandtl's theory completed with Oswald's efficiency number.

$$C_{L_\alpha} = \frac{C_{l_\alpha}}{1 + \frac{C_{l_\alpha}}{\pi AR}} \frac{1}{1+\delta} \tag{3.3}$$

Knowing that $AR = b^2 S = 10$, the necessary δ is obtainable from the "taper ratio versus δ" plot appearing in Enrique Ortega's finite wing theory book [12] (Figure 3.2).

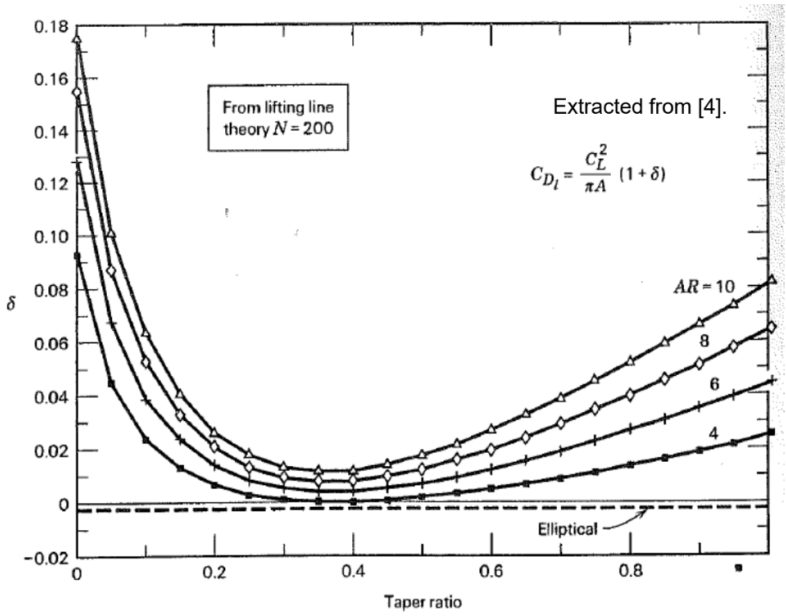

Figure 3.2: Plot of wing's AR, taper ratio versus δ.

Being the taper ratio 1 in the aircraft, the δ of it is $\delta = 0.08$. To obtain de C_{l_α} of the airfoil Xfoil simulations were performed. For this case, the used airfoil is a six digit $NACA\,63_1412$. This selection is based on the popularity of these airfoil type on similar aircraft. In addition, the favourable aerodynamic characteristics (constant load over the extrados and low drag ratio) are a key factor for the selection too.

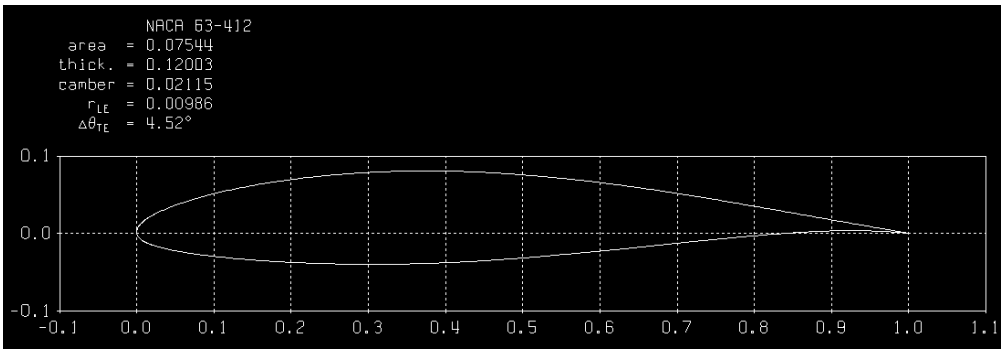

Figure 3.3: $NACA\,63_1412$ point distribution.

For the simulation, the chosen parameters are a viscous simulation and $Re = 6x10^6$, as the chord is known and the TO velocity is expected to be around 45-50. This results in, the polar graphics for the C_l *versus* α (Figure 3.4) and C_l *versus* C_d (Figure 3.5) graphs and various data are obtained 3.1.

However, for this wing configuration with an $\alpha = 2.5°$, the obtained TO velocity is $U_\infty = 77\,m/s$. This velocity is interpreted to be excessive for its MTOW. Therefore a 10° TE flap configuration is considered (Figure 3.6).

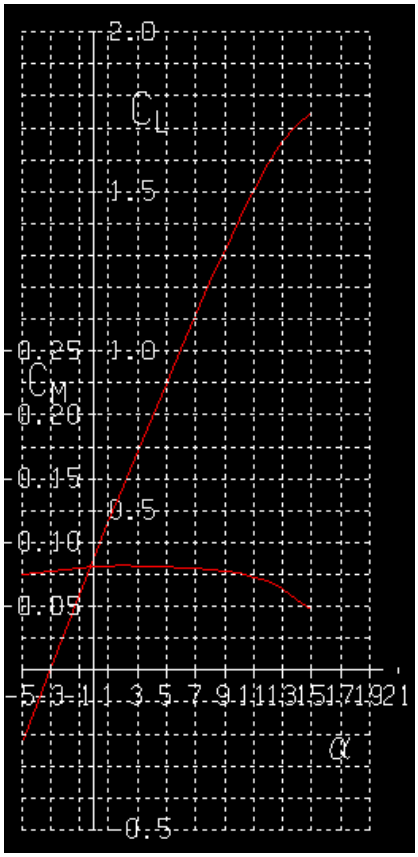

Figure 3.4: C_l versus α.

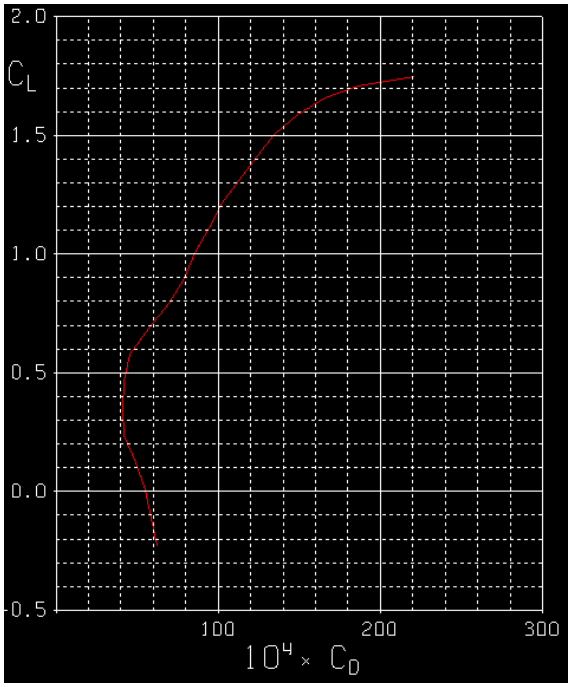

Figure 3.5: C_L versus C_D.

Parameters	Value
α_0	$-2.95°$
C_{l_α}	5.714
C_{d0}	0.00552

Table 3.1: Aircraft wing parameters.

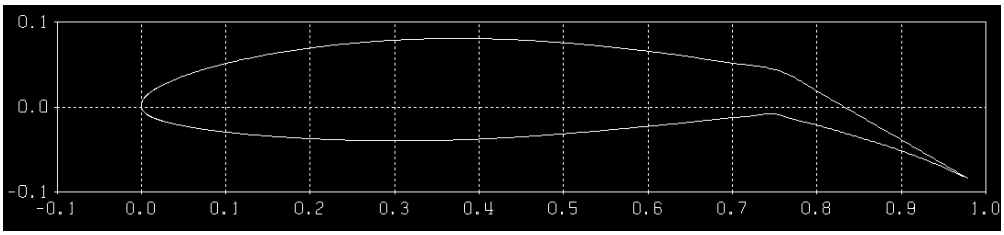

Figure 3.6: *NACA* 63_1412 point distribution with a $20°$ TE flap.

The new configuration being a TE hinge flap, maintains a linear slope and the curve moves to the left, reducing the zero lift and stall AoA. However, as the flap increases the curvature of the foil, the parasitic drag factor increases (Figures 3.7 and 3.8).

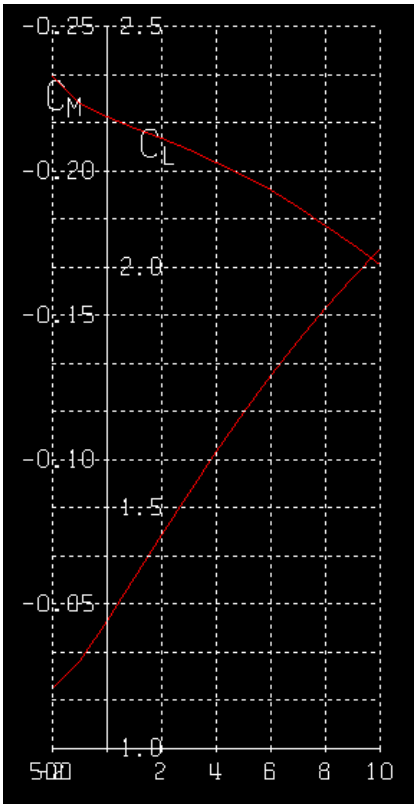

Figure 3.7: C_l versus α with a TE flap.

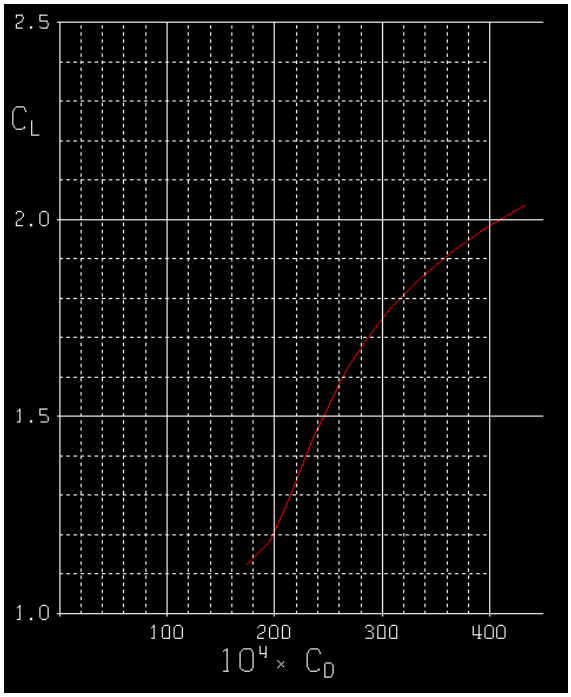

Figure 3.8: C_L versus C_D with a TE flap.

Parameters	Value
α_0	$-16.80°$
C_{l_α}	4.971
C_{d0}	0.00821

Table 3.2: Aircraft wing with flap parameters.

The new parameters appear to be better for a slower TO speed. After coding the equations in MatLab, the obtained speed is $U_\infty = 42\, m/s$ which is an acceptable speed for this type of aircraft.

However, a total dynamic performance study would be key for a better understanding of the TO phase. The missing dynamic equation is the one of the horizontal axis.

$$\vec{T} - \vec{D} - \vec{R} = m \cdot \vec{a} \tag{3.4}$$

Where each term is represented by the following equations:

$$T = \frac{T_{static} - 2TU_{MAX}}{U_{MAX}^2} V^2 + \frac{3TU_{MAX} - 2T_{static}}{U_{MAX}} V + T_{static} \tag{3.5}$$

Being a propeller driven aircraft the power is not ideally transferred by it and a efficiency factor of $\eta_p = 0.8$ must be assumed.

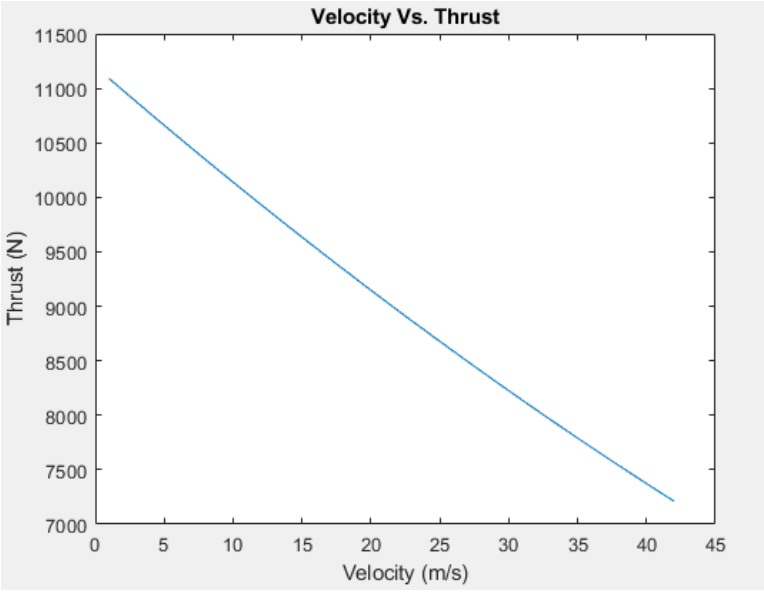

Figure 3.9: Thrust variation over velocity.

It is observable that the available thrust drastically reduces as velocity increases, which can be a critical part for the TO performance, as it fights against all the generated drag.

$$D = C_D \frac{1}{2}\rho U_\infty^2 S = \left[\frac{C_L^2}{\pi AR}\frac{1}{1+\delta} + C_{d0}\right]\frac{1}{2}\rho U_\infty^2 S \tag{3.6}$$

For the aerodynamic drag equation all the variables are known from the vertical dynamic equations as well as from the airfoil results.

$$R = C_R(C_U)\rho_w g B_f^3 \tag{3.7}$$

The hull drag differs from the previous one as the new medium is water. B_f is the hull width whose value is $B_f = 1.75\,m$. The behaviour of C_R is dependent on the velocity coefficient $C_U = \frac{U_\infty}{\sqrt{gB_f}}$, which is graphically represented on the TN2481 [20]. For a better development of its dynamics, an empirical Gaussian function curve fitting has been obtained by Sinchai Chinvorarat [5].

$$C_R = 0.05789e^{-(\frac{C_U-1.907}{0.7561})^2} + 0.0273e^{-(\frac{C_U-1.347}{0.2536})^2} - 0.3322e^{-(\frac{C_U-23.41}{11.74})^2} + 0.07924e^{-(\frac{C_U-3.227}{1.951})^2} \tag{3.8}$$

As both drag forces are an impeding force, the sum of both forces will be plotted for the dynamic solver (Figure 3.10.

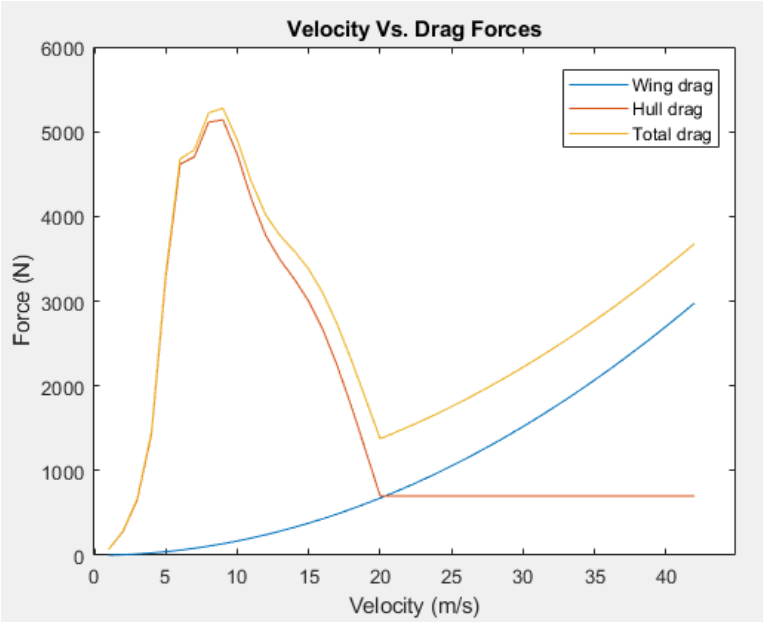

Figure 3.10: Aerodynamic and hull drag with the corresponding resultant of both.

As the hull drag graph and plot are limited to a $C_U = 5$ and the aircraft almost doubles it, it is assumed that the aircraft at $U_\infty = 20\, m/s$ starts hydroplaning. Thus, maintaining the drag constant until TO.

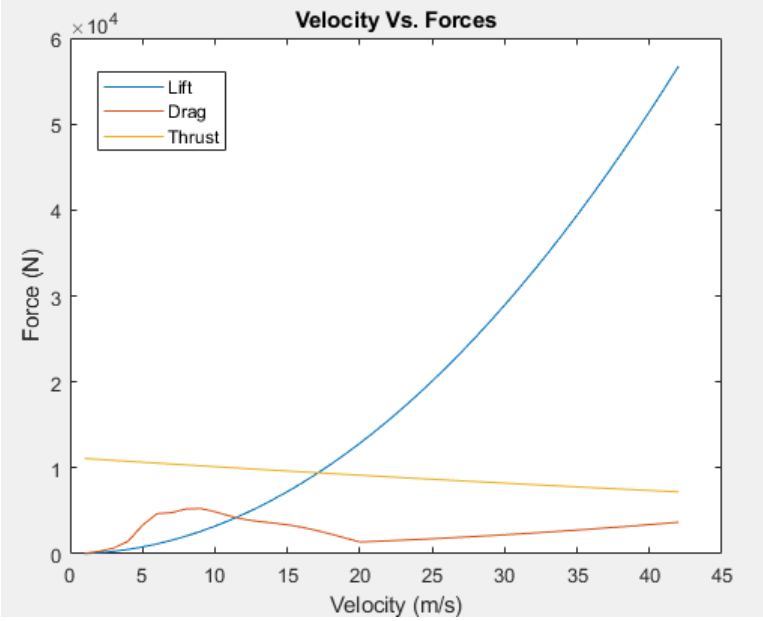

Figure 3.11: All the forces against the velocity.

On this graph (Figure 3.11) it can clearly be seen that the lift out performs the drag forces, reaching a $L/D \simeq 18$.

For the case of the empennage surface, the selected airfoil is a symmetric four digit NACA airfoil (Figure 3.12). This type of profile is ideal for a preliminary study, as at a zero AoA no lift is generated and the drag will be minimum. Thus, the forces of the empennage are not taken into account because the sole force is the drag and it has no great effect on the performance.

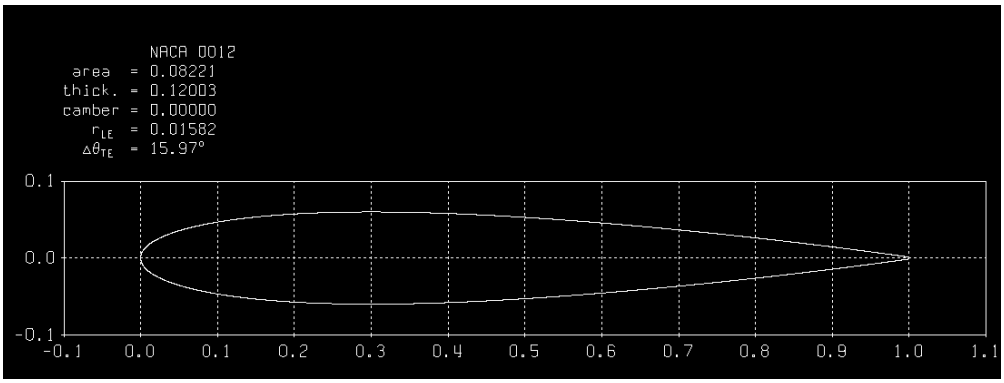

Figure 3.12: The empennage's wing profile *NACA* 0012 point distribution.

Even if the Figure 3.11 is useful to understand how speed affects on the plane's dynamics, a graph of the forces dependent of the time has a better use for comparing between models. For this initial model the obtained conclusion is that the aircraft takes off in 40 seconds.

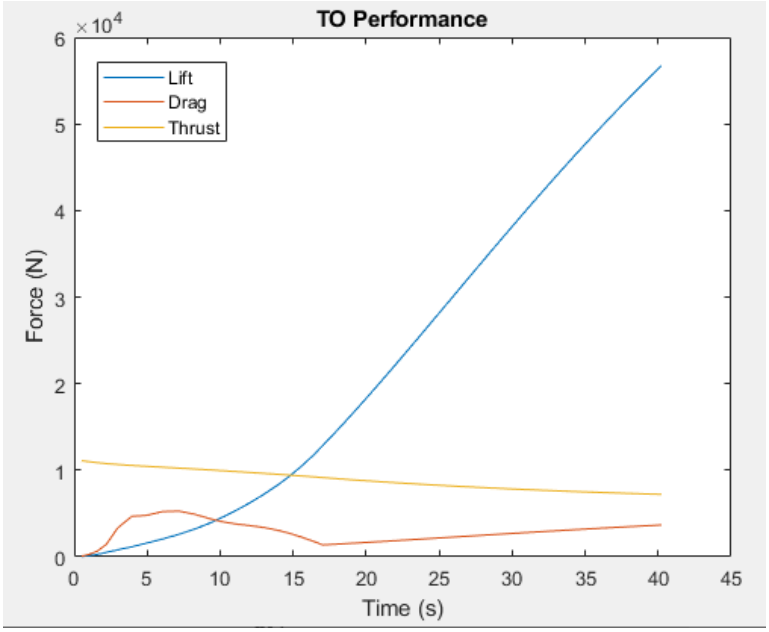

Figure 3.13: The TO performance for the amphibian aircraft without a hydrofoil device.

3.2 Hydrofoil Design

For the design of the wing it is necessary to set the profile's dimensions. As the studied foils are both based on the same principle, their defining equation only depends on A_1. Therefore, using the definition of $C_{l,d}$ A_1 can be obtained. Being water much denser than air, the generated lift at the same speed is much higher. As a consequence the used value is $C_{l,d} = 0.45$ and A_1 for J3T and J5T are the following respectively:

$$C_{l,d} = \frac{3\pi A_1}{4} \rightarrow A_{1,3} = \frac{4C_{l,d}}{3\pi} = 0.191$$

$$C_{l,d} = \frac{5\pi A_1}{6} \rightarrow A_{1,5} = \frac{6C_{l,d}}{5\pi} = 0.172$$

Finally obtaining the values for the two intrados:

$$\frac{y}{c} = \frac{0.191}{10}\left[5\frac{x}{c} - 20\left(\frac{x}{c}\right)^{\frac{3}{2}} + 80\left(\frac{x}{c}\right)^{2} - 64\left(\frac{x}{c}\right)^{\frac{5}{2}}\right] \tag{3.9}$$

$$\frac{y}{c} = \frac{0.172}{315}\left[210\frac{x}{c} - 2,240\left(\frac{x}{c}\right)^{\frac{3}{2}} + 12,600\left(\frac{x}{c}\right)^{2} - 30,912\left(\frac{x}{c}\right)^{\frac{5}{2}} + 35,840\left(\frac{x}{c}\right)^{3} - 15,360\left(\frac{x}{c}\right)^{\frac{7}{2}}\right] \tag{3.10}$$

For the extrados, initially a flat plane will be chosen. Its geometry will be modified for a better cavitation by trial and error on OpenFOAM.

3.3 Preprocessing

In order to begin the simulation, first, the meshing must be done. The main geometry of the control volume is a rectangular parallelepiped. The height of the rectangle is $h = 15c$ and the length is $l = 22c$, to obtain the development of the flow throughout the volume. Although the simulation is bi-dimensional, the meshing must be three-dimensional because of the nature of the CFD. Thus a relatively thin width has been selected, 0.1 m wide (Figure 3.14).

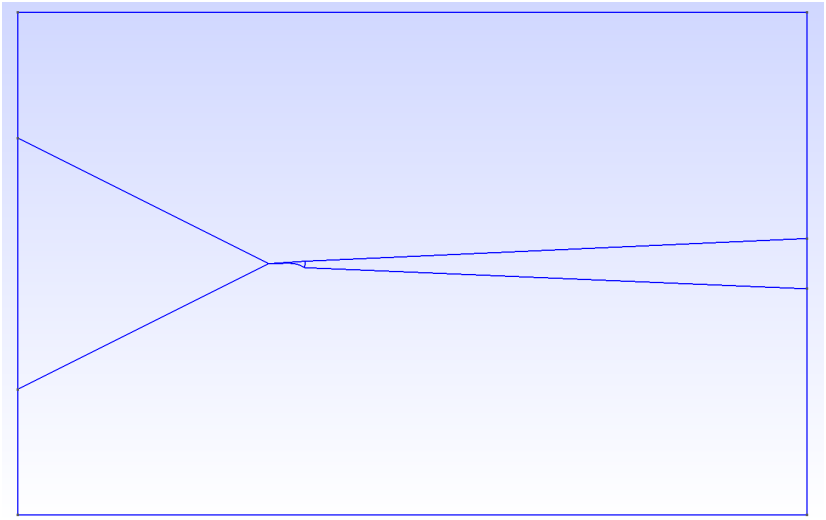

Figure 3.14: Plan view of the control volume.

Once the control volume is defined, the meshing is applied. For this case, in order to obtain an accurate solution near the foil, the area of the cell is $6.245x10^{-6}\,m^2$. In comparison, for the cells near the volume surface this area increases up to $0.194\,m^2$. In addition, the meshing geometry is unstructured with prism cells for a faster simulation (Figure 3.15). This cell geometry is a compromise between the run-time and the simulation quality.

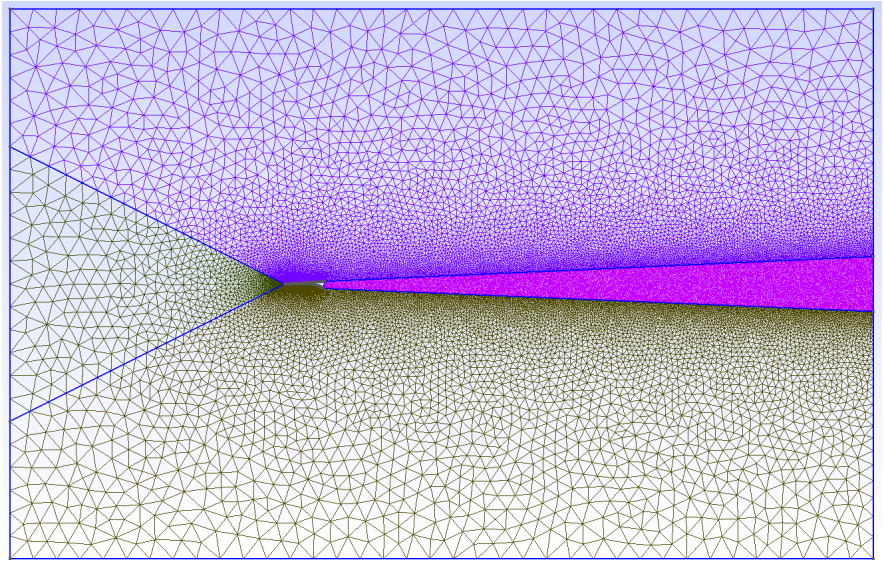

Figure 3.15: Meshing of the control volume.

A structured total or even partial hexahedral meshing would improve the overall meshing quality as the aspect-ratio, skewness and orthogonality would be strictly defined and therefore reduced. However, this would take a great amount of time for just a preliminary study where the objective is to get an idea of the viability of the project.

In order to solve the CFD simulation, surfaces of the control volume and the hydrofoil must be defined. The surfaces from whom the flow will enter are defined as inlet and outlet respectively. The front and back surfaces (the largest ones) are defined as empty, for the objective is to resemble a 2D flow study where finite wing phenomena will not happen. The top and bottom surfaces work as symmetry planes, which imitates the behaviour of an infinite flow volume. Finally, the hydrofoil surface is defined as wall, therefore the flow will interpret the surface as an object.

3.3.1 CavitatingFoam

It is clear that the flow case is going to be an incompressible and turbulent flow. But the most used solvers such as pimpleFoam, pisoFoam and simpleFoam are not capable to model the cavitating flow that occurs on a SC foil. For this type of cases there is already a standard solver known as cavitatingFoam. This solver is generally used for throttle body flows, but it is useful for a hydrofoil.

The initial conditions are similar to a simpleFoam (RANS) solver case with additional conditions: velocity, pressure, density, turbulent kinetic energy (k), turbulent viscosity (ν_t), specific turbulent dissipation rate (ω) and the vapour ratio (α_{vap}).

- U: Being a uniform stationary field, the velocity throughout all the control volume is initially constant and for the preliminary study $U_\infty = 20\,m/s$.
- P: Following the same principle, the internal pressure will be assumed to be constant in the control volume. $P = 38847.6\,Pa$ which is equal to being two meters deep in the water.
- ρ: As the used fluid is water, $\rho = 1000\,kg/m^3$.
- k: In order to obtain its value, it is necessary to calculate its variables:

$$k = \frac{3}{2}(UI)^2 \tag{3.11}$$

Where U is the average velocity of the flow with an initial value of $25\,m/s$ for initial margins and I is the turbulence intensity, dependent on U and the hydraulic diameter ($dh = 0.199\,m$).

$$I = 0.16 Re_{dh}^{-\frac{1}{8}} = 0.023 \tag{3.12}$$

After defining the variables the obtained turbulent kinetic energy for this flow is $k = 0.496$.

- ω: This value is defined by the following equation, where $l = 0.07dh = 0.014$ is known as the turbulence length scale.

$$\omega = \frac{\sqrt{k}}{l} = 50.305 \tag{3.13}$$

- ν_t: The turbulent viscosity is dependent on the turbulent kinetic energy and the specific turbulent dissipation rate.

$$\nu_t = \frac{k}{\omega} = 0.01 \tag{3.14}$$

- α_{vap}: For the case of this internal field no initial vapour is desired, therefore is zero.

Once the initial conditions are defined, the time control directory must be filled. The two key defining parameters are the stopAt time and deltaT. The first term must be defined to be as large as possible to obtain a fully developed flow, for this case a value of $stopAt = 0.8\,s$ has been defined. The latter one must be defined in order to obtain convergence for each time step. This parameter can be determined by the Courant number:

$$Co = \frac{\delta t|U|}{\delta x} \rightarrow \delta t = \frac{Co\delta x}{|U|} = 0.000008\,s \tag{3.15}$$

For the sake of convergence between the different hydrofoil designs, the used deltaT is $\delta t = 0.000001\,s$. Finally, every $0.01\,s$ a control case is written into the directory in order to observe the development of said flow.

The last steps to end the preprocessing phase are to define thermodynamic and transport properties of the fluid. For this study case, where water is the medium, the properties are the dynamic viscosity, density, kinematic viscosity, the derivative of density in respect with the pressure (psi) and the saturation pressure; all for liquid and vapour states (Figure 3.3).

Properties	Value
μ_l	$1.005x10^{-}3$
μ_v	$9.544x10^{-}6$
ρ_l	1000
ρ_v	0.017
ρ_{min}	0.01
ν_l	$1.005x10^{-}6$
ν_v	$5.614x10^{-}4$
psi_l	$7.316x10^{-}6$
psi_v	$5.553x10^{-}6$
p_{sat}	2339.3

Table 3.3: Thermodynamic and transport properties of water in liquid an vapour states.

3.4 J3T Hydrofoil Design

Once the intrados is defined, the initial model has a straight line as an extrados (Figure 3.16). Although simple, it will offer a base for future variations. On the other hand, the chord of the hydrofoil is defined to be $c = 1\,m$. The main reason is that the sought results are the force coefficients, and a simple value will be easier to calculate. The design velocity will be $U = 20\,m/s$. This way the amphibian aircraft can be lifted from water far earlier than if the design velocity was chosen to be $U = 45\,m/s$.

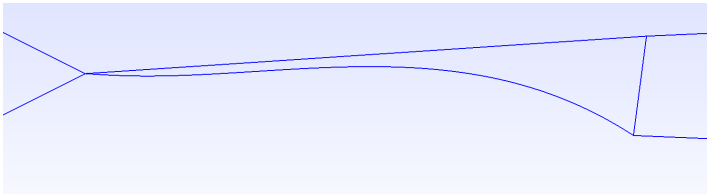

Figure 3.16: Initial hydrofoil.

After the simulation is done the key points of interest are the section L, D, their ratio and the vapour ratio, which indicates the cavitation phenomenon.

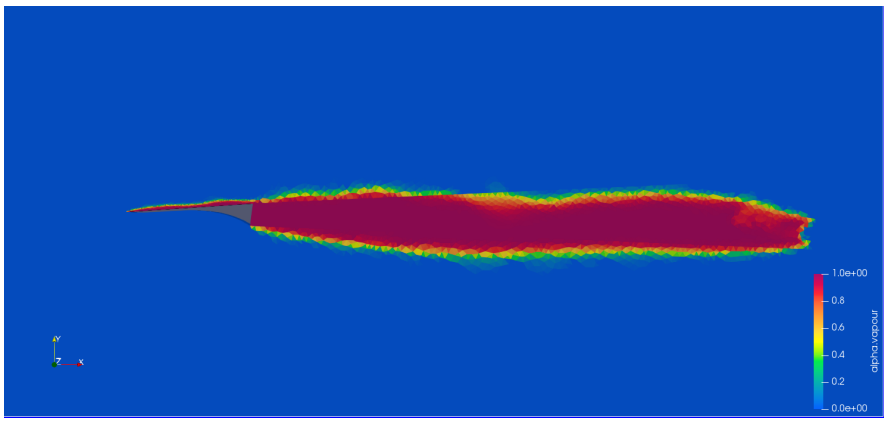

Figure 3.17: α_{vap} of the initial design.

L	12440.5 N
D	1470.19 N
L/D	8.46

Table 3.4: Aerodynamic forces of the initial hydrofoil.

As it can be seen on FIgure 3.17, this first design does develop cavitation, obtaining a fully ventilated cavitation. On the other hand, the cavitating flow over the extrados does not develop smoothly, a height bump can be clearly seen at $0.6 \cdot c$ which then gets close to the surface at the TE. This could be a factor for the efficiency of the foil being $L/D \simeq 8.46$.

3.4.1 First Extrados Variation

When seeking greater cavitation flow, acceleration is needed as pressure will be proportionally reduced. This velocity gradient can be obtained via a circular extrados. The parametrization of the designed extrados is presented on (3.16), as well as the foil geometry (Figure 3.18).

$$\left(\frac{x}{c} - 1.5\right)^2 + \left(\frac{y}{c} + 5.5\right)^2 = 32.5 \tag{3.16}$$

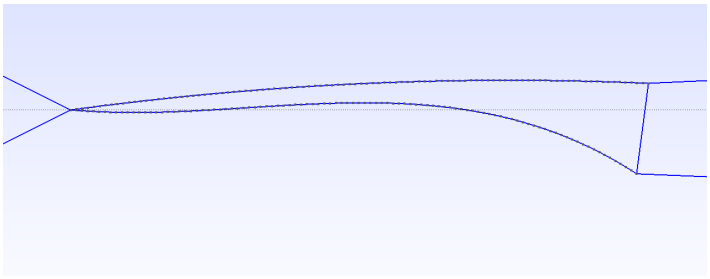

Figure 3.18: Circular extrados hydrofoil.

On this first variation the cavitation around the hydrofoil is smoother (Figure 3.19). This can be interpreted as less disturbance of the flow and therefore the reason behind the drag reduction in comparison to the previous one.

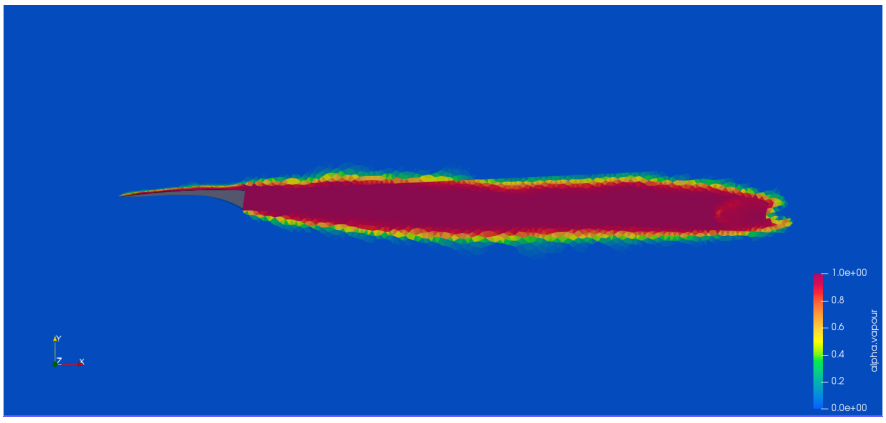

Figure 3.19: α_{vap} for the circular extrados.

L	12140.5 N
D	1457.72 N
L/D	8.33

Table 3.5: Aerodynamic forces of the first variation hydrofoil.

However, for this first variation no performance improvement can be obtained. Although reducing the drag around the hydrofoil, the lift also is decreased, obtaining a lower efficiency

factor than the initial design. Nevertheless, it is possible that a non constant curvature could improve said performance.

3.4.2 Second Extrados Variation

A typical non-constant curve for airfoils is the one generated by parabolas (Figure 3.17). Based on this idea, the main objective was to obtain a higher curvature on the foil, as well as having the maximum height at the second half of the hydrofoil.

$$\frac{y}{c} = 0.15\left(\frac{x}{c} - 1\right)^2 - 0.15 \tag{3.17}$$

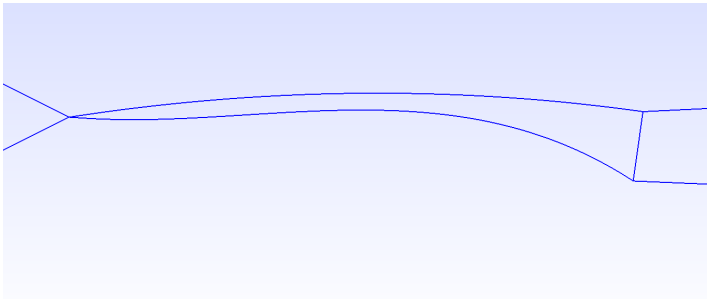

Figure 3.20: Parabolic extrados hydrofoil.

On this second variation the cavitating flow maintains a fairly linear development throughout the hydrofoil (Figure 3.21). Nevertheless, the cavitation increases its height due to the negative slope, possibly creating some turbulence. This could be the reason to the increment on D. On the other hand, this is the hydrofoil with the highest lift generation and that should be taken into account.

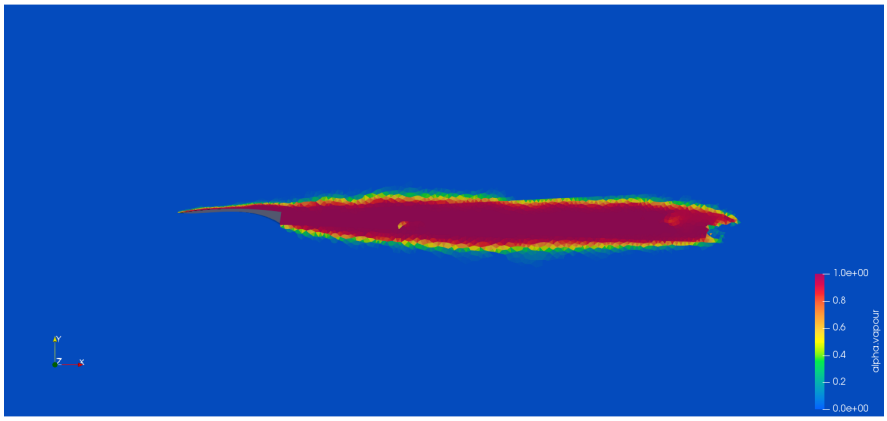

Figure 3.21: α_{vap} for the parabolic extrados.

L	12582.3 N
D	1491.3 N
L/D	8.43

Table 3.6: Aerodynamic forces of the second hydrofoil variation.

3.4.3 Third Extrados Variation

A variation to obtain a higher gain on the performance was to use the parabolic equations that define a four digit NACA airfoil, as it is designed specifically for lifting devices. These airfoil's mean camber are designed by using two parabolas which depend on the maximum camber and its relative position to the chord. For this case, only the first parabola is used to define the extrados of the hydrofoil (3.18)(Figure 3.22).

$$\frac{y}{c} = 1\frac{x}{0.8^2 c}\left(1.6 - \frac{x}{1.5c}\right) \tag{3.18}$$

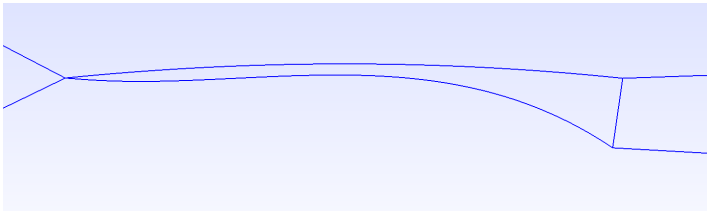

Figure 3.22: NACA based extrados hydrofoil.

Once again the cavitation does develop linearly through the hydrofoil and the drag force is quite similar to the previous ones (Figure 3.23). It is clear that a quadratic extrados variation has not enough capability to make a difference in the performance.

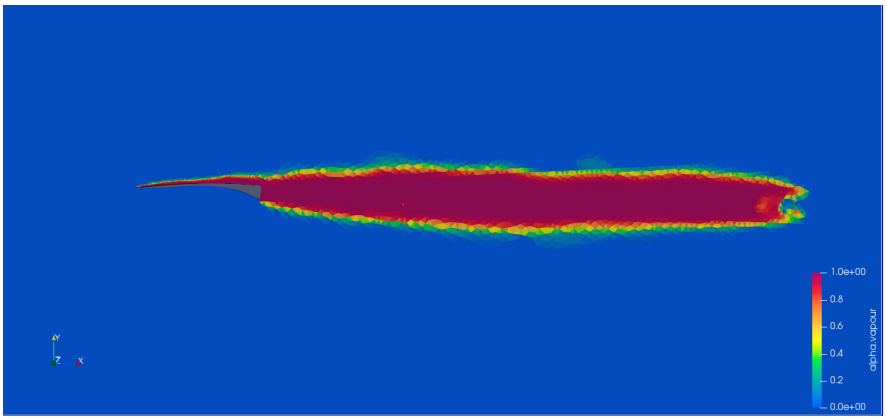

Figure 3.23: α_{vap} for the NACA extrados.

L	12393 N
D	1468.77 N
L/D	8.44

Table 3.7: Aerodynamic forces of the NACA hydrofoil variation.

3.4.4 Fourth Extrados Variation

As a last try an inversely quadratic equation is tried (3.19). The idea behind this geometry is to generate a higher flow deflection at the LE in order to force a higher cavitation volume. This will probably generate a higher drag force in expense of an improvement of lift force.

$$\frac{y}{c} = 0.2\sqrt{\frac{x}{c} + 0.01} - 0.02 \tag{3.19}$$

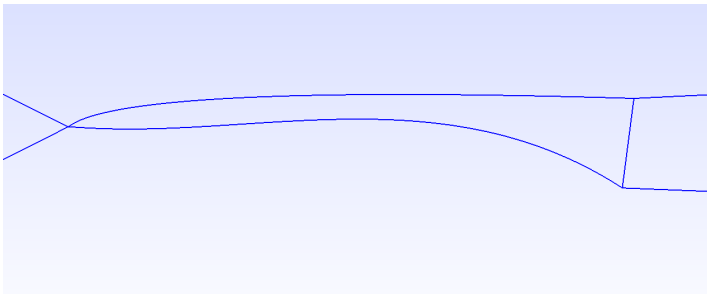

Figure 3.24: Inversely quadratic extrados hydrofoil.

Although cavitation does develop on the hydrofoil, its height does not increase in any way (Figure 3.25). As a mater of fact, the cavitation begins later on the extrados (around 0.05 c), further reducing the lifting force. This delay on the cavitation phenomenon increases the drag force too. Definitely this extrados design is not suitable for the objective of the study.

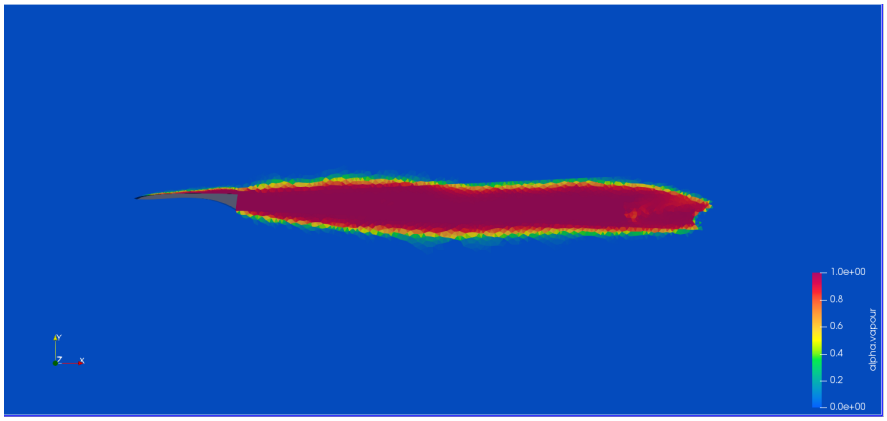

Figure 3.25: α_{vap} for the inversely quadratic extrados.

L	11983 N
D	1589.1 N
L/D	7.49

Table 3.8: Aerodynamic forces of the inversely quadratic hydrofoil variation.

3.4.5 Hydrofoil Design Selection

It is clear that for a fully ventilated hydrofoil, as the one used on this study, the extrados geometry changes does not generate great improvement on the forces. In fact, efficiency can be greatly reduced by the changes on the extrados.

Three extrados designs are the ones with the highest L/D ratio: the initial design, the second variation (parabolic) and the third variation (NACA). All of them have a efficiency ratio around 8.45 with a deviation below 5%. At first sight, the initial design could be the best option as for a simpler geometry similar lift can be generated. However, certain extrados curvature could be useful to improve the lift performance at low speeds. Therefore, the second variation is the one chosen, for it presents the greatest curvature.

After selecting the hydrofoil design and the general wing geometry, a final wing parametrization will be made. In order to parametrize said wing, the lift and drag coefficients of the hydrofoil must be defined from the obtained force values from the CFD ($S = 0.1\ m^2$ is the surface of the foil in openFOAM):

$$C_{l_h} = \frac{L_h}{\frac{1}{2}\rho_w U_\infty^2 S} = 0.629$$

$$C_{d_h} = \frac{D_h}{\frac{1}{2}\rho_w U_\infty^2 S} = 0.075$$

Cavitation is a relevant factor for the performance of the wing, which is dependent on the velocity of the flow. Thus, a number of extra CFD simulations will be carried out at various velocities (10, 30 and 40 m/s) to understand the performance of the hydrofoil during take off.

- U = 10 m/s: On this flow regime the cavitation develops through the entire hydrofoil. However, it suddenly closes at the TE. This may be the reason to generate a relatively higher C_d even with such a low velocity (Figure 3.26).

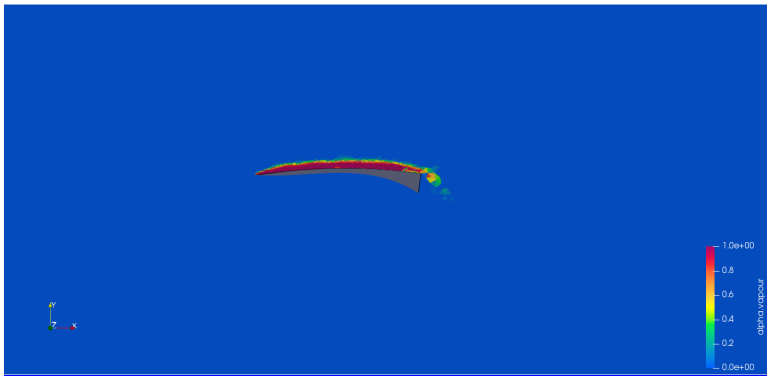

Figure 3.26: α_{vap} for $U = 10\,m/s$.

- U = 30 m/s: After the design velocity, it is clear that the overall hydrofoil performance decreases. The main concern resides on the drag coefficient, as it stays fairly constant for a higher velocity (Figure 3.27).

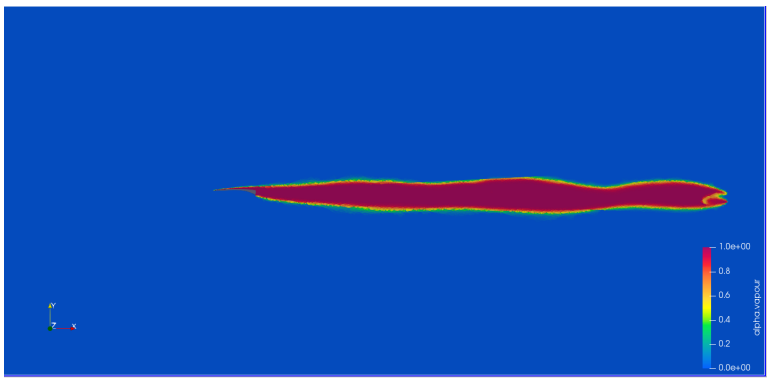

Figure 3.27: α_{vap} for $U = 30\,m/s$.

- U = 40 m/s: For this last flow regime the decrease of performance stays constant (Figure 3.28).

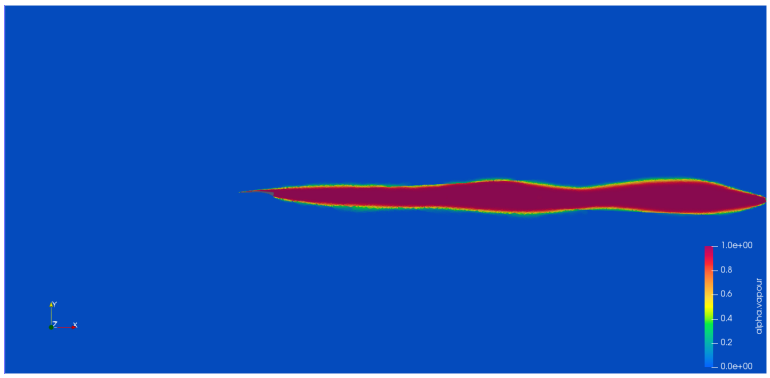

Figure 3.28: α_{vap} for $U = 40\,m/s$.

Velocity (m/s)	C_{l_h}	C_{d_h}	$\frac{C_{l_h}}{C_{d_h}}$
10	1.515	0.128	11.87
20	0.629	0.075	8.44
30	0.593	0.071	8.30
40	0.559	0.068	8.20

Table 3.9: Hydrofoil performance throughout various velocities.

Due to the lack of points, a linear approximation has been made for each speed difference. Ideally a cubic approximation could be better but, it would require a great amount of time for said CFD simulation.

3.5 Hydrowing Design

To begin the design of the wing a configuration must be chosen. As being on a preliminary state, a simple wing configuration is desired. For this design the selected velocity is 20 m/s, where the wing is able to generate a quarter of the necessary force for lift off. It can be concluded that the control surfaces are responsive at this point, therefore a single hydrofoil Grunberg system is chosen.

Being that the speed of sound in water is higher than in air, the wing is going to be designed for a low-subsonic flow regime. This translates to not adding wing sweep back. Moreover, as the study is seeking a simple initial design, no aerodynamic nor geometric twist is contemplated. Finally, even if a dihedral would be usefull for coupling with the hull after TO and increase stability, it would reduce in a extent the efficiency that can be key for this preliminary study. Thus, no wing dihedral will be applied.

When searching for parameters that could increase the efficiency of the wing, the AR and λ (taper ratio) are useful elements, as they do not require too much structural and engineering effort. Recalling the Figure 3.2 from Enrique Ortega's theory book [12], it is visible that the most efficient wing after the elliptical platform is the one with $AR = 4$ and $\lambda \simeq 0.35$.

As the coefficients are defined, the wing surface can be obtained. For the desired velocity, the lifting devices must be able to hold the gross weight of the airplane. From the initial model it is possible to obtain the generated lift by the wing for $U_\infty = 20\, m/s$ ($L = 12863.2\, N$).

$$L + L_h = MTOW \cdot g \rightarrow L_h = 55622.7 - 12863.2 = 42759.5\, N$$

The selected hydrofoil is not normalized, as it could be a NACA airfoil or low Re hydrofoil, there are not enough resources to do a complete hydrofoil study. Thus, no real wing lift approximations can be made due to the lack of performance data for different AoA. As a consequence the only way of dimensioning the hydrowing is by reusing the C_l expression from before (2.8) and interpreting as an ideal solution.

$$S_h = \frac{L_h}{\frac{1}{2}\rho_w U_\infty^2 C_{l_h}} = \frac{42759.5}{\frac{1}{2}1000 \cdot 20^2 \cdot 0.629} = 0.34\, m^2$$

After defining the wing it is of great relevance to calculate the value of the hydrodynamic drag, which is defined at the state of the art (2.14). For the value of C_{D_0} it is used the expression found on the guidebook "Aircraft Design, a Systems Engineering Approach" [16]. However, as the real wing values can not be approximated, the ideal expressions are used:

$$\left(\frac{L}{D}\right)_{max} = \frac{1}{2\sqrt{kC_{D_{0_h}}}} \rightarrow C_{D_{0_h}} = \frac{\pi C_{D_h}^2}{C_{L_h}^2} \tag{3.20}$$

For the case of the C_{D_i} the known equation is used. Note that the constant k is used as a shortening of $k = \frac{1+\delta}{\pi AR}$.

$$C_{D_{i_h}} = kC_{l_h}^2 \tag{3.21}$$

Finally the drag value for the designed wing is:

$$D = (C_{D_{0_h}} + C_{D_{i_h}})\frac{1}{2}\rho_w U_\infty^2 S_h \tag{3.22}$$

Once the TO dynamics are updated for the hydrofoil device a new Matlab code is written to obtain the vertical forces (Figure 3.29), drag forces (Figure 3.30) and the totality of forces (Figure 3.31), all throughout the velocity values, this code is visible at the annex.

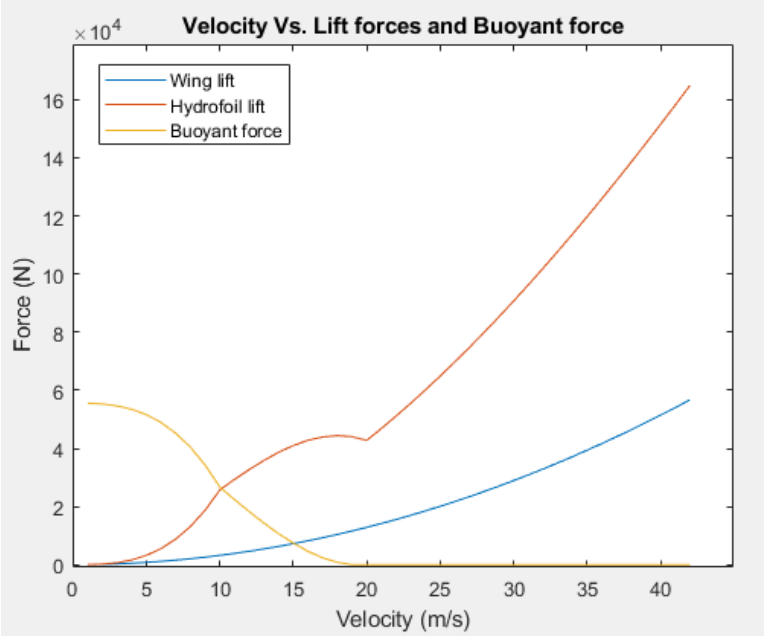

Figure 3.29: Vertical forces for different velocity values.

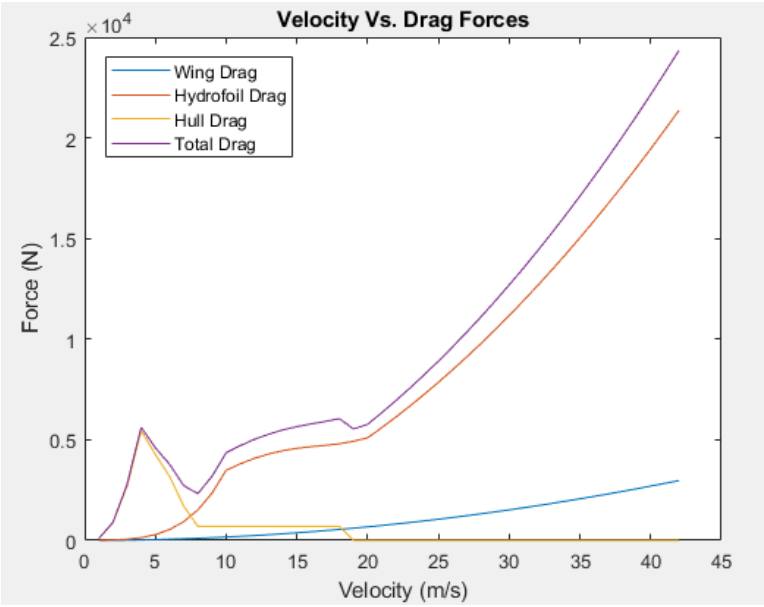

Figure 3.30: Drag forces for different velocity values.

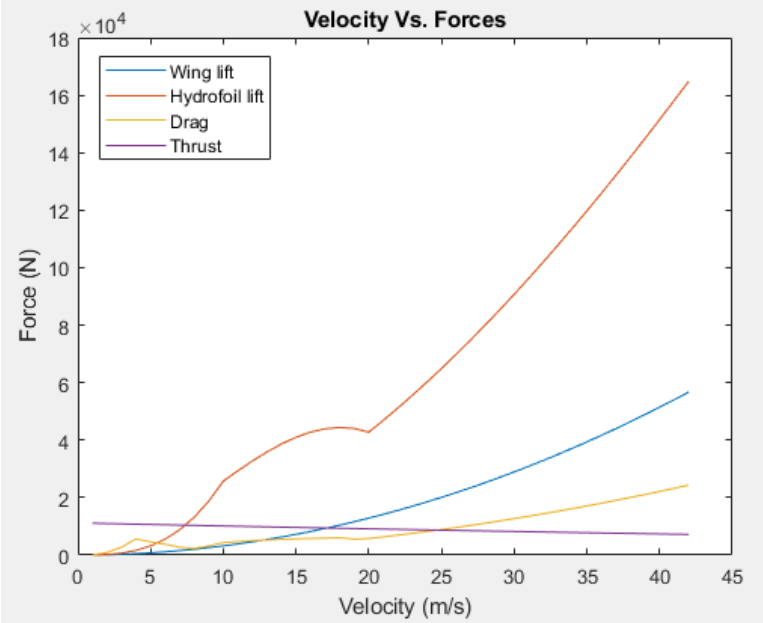

Figure 3.31: TO forces for the velocity values.

Although the lift force develops successfully through the TO run, the drag generated by the hydrofoil increases drastically, making TO velocity impossible to obtain. The only variable left for the geometric definition is the hydrofoils surface, which is defined for $U_\infty = 20\, m/s$. Another option is to define the surface for $U_\infty = 35\, m/s$ ($L = 39390\, N$).

$$L + L_h = MTOW \cdot g \rightarrow L_h = 55622.7 - 39390 = 1632.7\, N$$

$$S_h = \frac{L_h}{\frac{1}{2}\rho_w U_\infty^2 C_l} = \frac{1632.7}{\frac{1}{2}1000 \cdot 35^2 \cdot 0.629} = 0.046\, m^2$$

Once the new hydrowing surface is defined and code rerun, it is clear that lift off can be obtained (Figure 3.34).

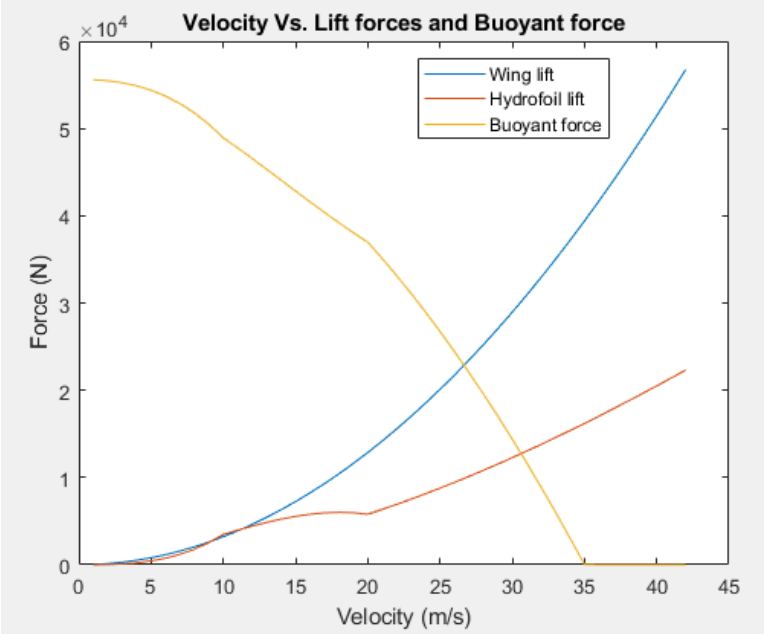

Figure 3.32: Vertical forces for different velocity values.

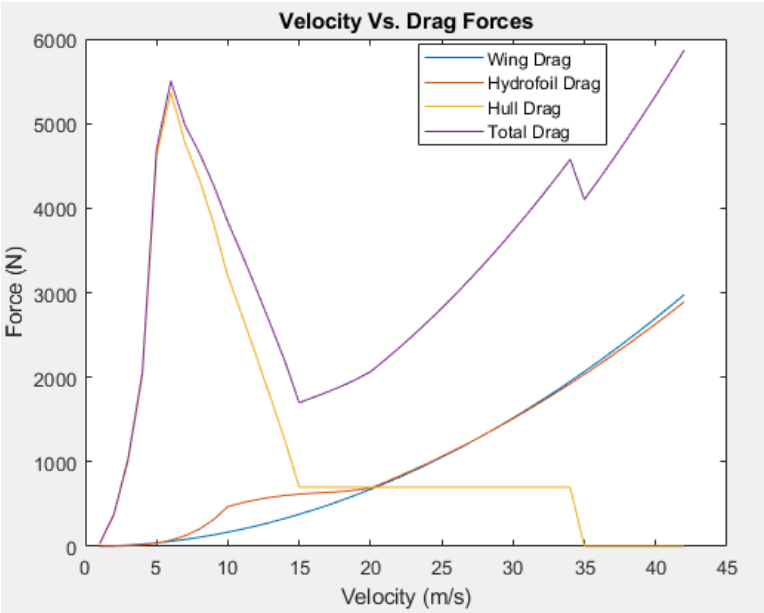

Figure 3.33: Drag forces for different velocity values.

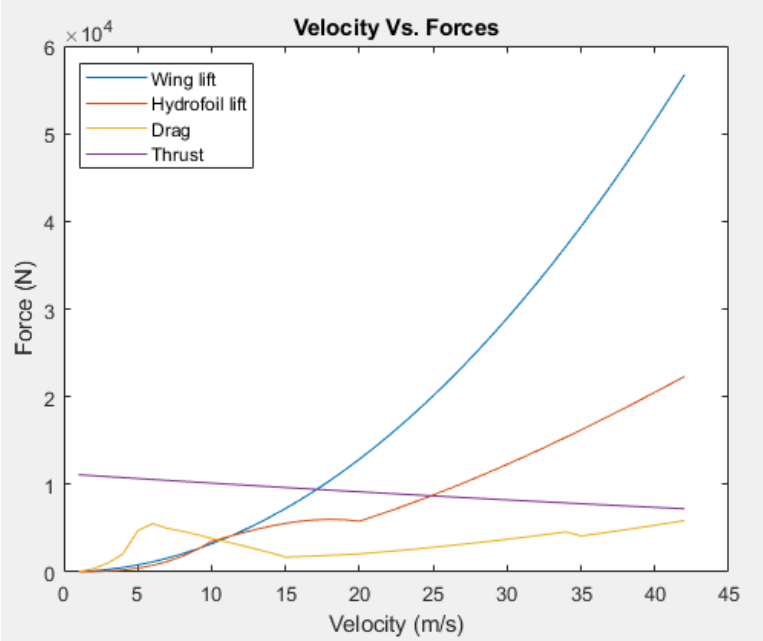

Figure 3.34: TO forces for the velocity values.

However, performing the TO run in function of time shows that it is going to take longer to lift off than without a hydrofoil device (Figure 3.35). Specifically 12.1 *s* longer and therefore, a longer much longer distance.

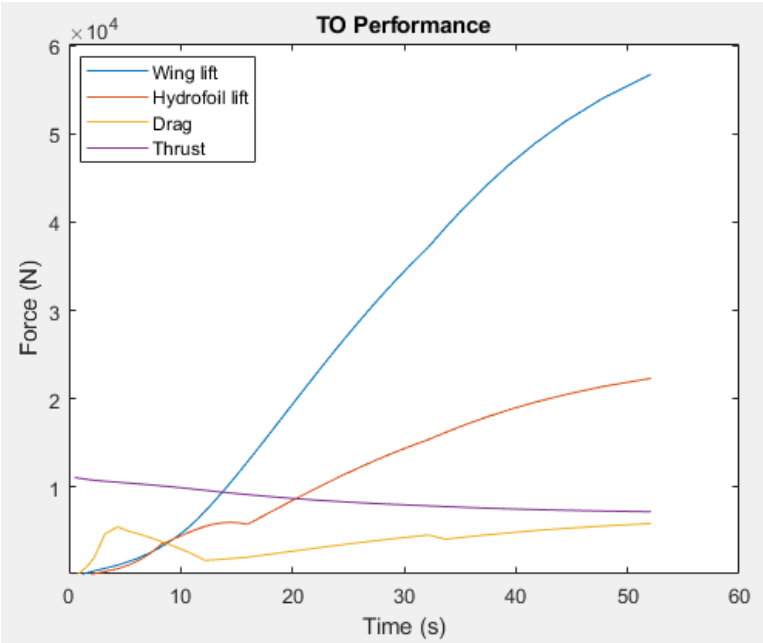

Figure 3.35: TO performance.

A last option is that the new surface defining criteria is: having a shorter TO time. This is obtained by trial an error but, it is known that the surface must be at least smaller than

$S_h = 0.046\,m^2$. After several attempts no hydrowing surface can be obtained that can improve the TO run of the non hydrofoil aircraft. The main reason behind this statement is that the surface being smaller than $Sh = 0.005\,m^2$ can not reduce the drag neither generate enough lift to rise the aircraft. Achieving a performance similar to the initial model.

It is clear that the designed hydrofoil is not performing as expected. In addition a small surface as $S_h = 0.05\,m^2$ translates to a immense wing load, which can be a major structural impediment. On the other hand, a greater surface generates an unacceptable amount of drag that can directly out perform the total thrust.

4 Final Design

4.0.1 Wing

As before mentioned the final wing platform has important structural and performance drawbacks. The physical feasibility of the hydrofoil device must be discarded.

4.0.2 Material selection

After completely defining the hydrofoil device for the amphibian aircraft, an initial material selection is made as it could be helpful for future studies that approach the problem from another point of view. Although no structural study has been made, it is of great relevance to compare the different available material options. The most common materials for aircraft are quite similar to the ones used on water based vehicles. The most common materials being steel [14], aluminium [15][21], FRP composites (carbon and glass) [1].

Material	Density (kg/m^3)	Traction resistance (MPa)	Young modulus (GPa)	Cost (€/kg)
Steel	7850	500	200	2
Aluminium	2700	500	75	2.5
CFRP composite	1600	3920	150	41
GFRP composite	1875	4580	86	30

Table 4.1: Material properties.

Once each material's properties are declared a comparison between them is made. This is done with the press method of selection. On this method each factor is relevance weighted and each material has a grade for its characteristics. Afterwards, the valuation and domination matrix are calculated in order to obtain the importance index. The reasoning behind the weighting of each characteristic is that the greatest concern of an aircraft is avoiding to gain a lot of mass. This is followed by the structural integrity of the device, which for this case is of great interest, as a relatively small surface will be experiencing a big fraction of the vehicle's weight. Finally, the cost is the least important one. This is because of the novelty of the technology which requires more advanced materials in order to ensure its success.

Criteria	Density (kg/m^3)	Traction resistance (MPa)	Young modulus (GPa)	Cost (€/kg)
Weight	35	25	25	15
Relative	0.35	0.25	0.25	0.15
Materials				
Steel	1	1	5	5
Aluminium	4	1	2	5
CFRP composite	5	4	4	1
GFRP composite	4.5	5	2.5	1.5
P_{max}	5	5	5	5

Table 4.2: Initial data.

0.07	0.05	0.25	0.15
0.28	0.05	0.1	0.15
0.35	0.2	0.2	0.03
0.315	0.25	0.125	0.045

0.000	0.15	0.17	0.23
0.21	0.000	0.12	0.105
0.43	0.32	0.000	0.11
0.445	0.26	0.065	0.000

Table 4.3: Valuation and domination matrices respectively.

As the press method shows, the greatest grade is obtained by the CFRP composite. Therefore this is the selected material for the hydrofoil device.

Steel	Aluminium	CFRP	GFRP
0.51	0.60	2.42	1.73

Table 4.4: Selection Results.

5 Economic Feasibility

Although the physical feasibility of a hydrofoil for amphibian aircraft has been rejected, its economic feasibility has been studied to, at least, confirm the feasibility from a business point of view. Initially, the venture opportunity must be financially modelled in order to obtain a break-even point.

The main goal is to achieve the level of revenue required to fulfil the return of the initial investment. In order to obtain this value, a study of the costs due to manufacturing and operations will be made.

5.0.1 Initial Investment

On this section the necessary initial asset for starting up the project is determined. The idea behind this is to approximate the expenses needed to do at least once to develop the project.

This estimation is made with the parametric Chilton method [8]. The method begins with the cost of the equipment needed which is later estimated considering a set of factors obtained from historical information (Figure 5.1). Initial value of **0.6M €** is estimated due to relative small size of the attachment in comparison to the aircraft.

Item	Factor	% of item
1. Delivered equipment cost	1.0	1
2. Installed equipment cost	1.43	1
(or directly from cost data)		
3. Process piping		
Type of plant		
Solid	0.07–0.10	2
Solids–fluid	0.10–0.30	2
Fluid	0.30–0.60	2
4. Instrumentation		
Amount		
None	0.03–0.05	2
Some	0.05–0.12	2
Extensive	0.12–0.20	2
5. Buildings and site development		
Type of plant		
Outdoor	0.10–0.30	2
Outdoor–indoor	0.20–0.60	2
Indoor	0.60–1.00	2
6. Auxiliaries		
Extent		
Existing	0	2
Minor addition	0–0.05	2
Major addition	0.05–0.75	2
New facilities	0.25–1.00	2
7. Outside lines		
Average length		
Short	0–0.05	2
Intermediate	0.05–0.15	2
Long	0.15–0.25	2
8. Total physical plant costs		
Σ of items 2–7		
9. Engineering and construction		
Complexity		
Simple	0.20–0.35	8
Difficult	0.35–0.60	8
10. Contingencies		
Process		
Firm	0.10–0.20	8
Subject to change	0.20–0.30	8
Speculative	0.30–0.50	8
11. Size factor		
Size of plant		
Large commercial unit >$10MM	0–0.05	8
Small commercial unit $0.5MM to $10MM	0.05–0.15	8
Experimental unit <$0.5MM	0.15–0.35	8
12. Total fixed plant cost (Σ items 8–11)		

Figure 5.1: Chilton factors.

Based on the factor values presented on this table the expenses of this project are calculated and gathered on the following table.

Item	Factor	% of Item	Value (€)
1	1.0	1	600 k
2	1.43	1	858 k
3	0.08	2	48 k
4	0.12	2	72 k
5	0.6	2	360 k
6	0.08	2	48 k
7	0.05	2	30 k
8			2.016 M
9	0.40	8	240 k
10	0.20	8	120 k
11	0.15	8	90 k
12			2.466 M

Table 5.1: Chilton method of the project.

The total initial cost of the facility and equipment is estimated to be **2.466 M €**.

5.0.2 Operational Cost

The RAND Corporation has a cost estimating model to predict ADC known as the DPCA. The variation of this model is defined by the following equation [8]:

$$ADC = H_E R_E + H_T R_T + H_M R_M + H_Q R_Q + C_D + C_F + C_M \tag{5.1}$$

where H refers to the necessary hours for each factor and R to the cost for said factors. For the sake of clarity, the models for the tasks are shown next:

1. Engineering Hours:
$$H_E = 5.18 W_e^{0.777} V^{0.894} Q^{0.163} \tag{5.2}$$

2. Tooling Hours:
$$H_T = 7.22 W_e^{0.777} V^{0.696} Q^{0.263} \tag{5.3}$$

3. Manufacturing Labour:
$$H_M = 10.5 W_e^{0.82} V^{0.484} Q^{0.641} \tag{5.4}$$

4. Quality Control:
$$H_Q = 0.133 H_M \tag{5.5}$$

5. Development-support Cost:
$$C_D = 67.4 W_e^{0.630} V^{1.3} \tag{5.6}$$

6. Manufacturing Materials:
$$C_M = 31.2 W_e^{0.921} V^{0.621} Q^{0.799} \tag{5.7}$$

Factor	Value
W_e (Weight)	15 (kg)
V (Maximum velocity)	42 (m/s)
Q (production quantity in 5 years)	12
R_E (Engineering cost)	128 (€)
R_T (Tooling cost)	132 (€)
R_Q (Quality cost)	121 (€)
R_M (Manufacturing cost)	110 (€)

Table 5.2: DPCA factors values.

After applying this model the development and procurement cost rises to **827.743 k €**.

5.0.3 Unit Selling Price

Being that amphibian aircraft are not so common in the sector as land based ones, the production of the device will be a small fraction of the total DHC-6 annual production (around 30 aircraft manufactured per year). On the other hand, being a new technology the price is based on the money charged for the installation of floats on smaller and similar aircraft (around **800 k €**), also taking into account the need of installing mechanisms and security aspects. Finally, an approximation of the sales evolution per year is made.

Year	0	1	2	3	4	5	6	7
Units sold	0	1	2	3	6	8	10	10

Table 5.3: Units sold per year.

5.0.4 Feasibility Study

After estimating various expenses calculation, the economic feasibility is going to be studied. The aim of this study is to determine the viability of the project. The full approximation calculation table is available at the annex.

5.0.4.1 Payback Period

This value is an initial approximation to the minimum required period to recover the investment. Its value is obtained by dividing the initial investment times the average **CF** (Cash Flow). First the EBITDA is calculated as a initial approach to the payback time, where the CF is simply the revenues. As a result, the **payback period value is 2 years and 8 months**.

For a better approximation the CF is updated by taking into account the discount rate of 7% ($k = 0.07$):

$$VP = \frac{CF_t}{(1+k)^t} \tag{5.8}$$

Where the new CF is the VP, CF_t is the cash flow at that year and t is the year. Once again calculating the average CF, the **updated payback time is 5 years**.

5.0.4.2 NPV

This value is the sum of cash inflows and outflows over a period of time. In this case the period of time is the defined seven years of the project. This value is an indicator of the viability of the project, where a positive value indicates that the investment may be advisable.

$$NPV = -C_0 + \sum_{t=1}^{7} \frac{C_t}{(1+k)^t} \tag{5.9}$$

The obtained value for this project at seven years is **NPV = 1.323 M €**.

5.0.4.3 IRR

The IRR is calculated to obtain the highest discount rate where the project still is advisable (NPV=0). It is expected that this value is going to be higher than the used for the initial approximation. The final calculation shows that **IRR = 0.104**, the value is definitely higher than k and the margin is of around 3%.

5.0.4.4 Break-Even Point

Finally, the break-even point is calculated in order to obtain the amount of manufactured products where the project is profitable. On this case the number of hydrofoil devices is 5.

5.0.4.5 Results

The unit selling price can not be better approximated as no similar implementation can be found, however it is still reasonable due to the novelty of the project. For the case of the payback period is around 2,7 to 5 years. The margin is quite great, but the upper limit is close to not being profitable, which is reflected on the NPV. Although the last year value is positive, this is the first year being positive. On the other hand, the IRR has a small margin as in other cases a margin of 8-10% are obtained. At last, the break-even point is a reasonable value.

All in all, the project seems feasible. The risks may appear greater than for traditional projects but, for a new technology, a higher profit can be gained.

6 Environmental Impact

The dimension of this project is not large, where no manufacturing processes are carried out. Nevertheless, it is still relevant to acknowledge the impact a preliminary study can have and the possible solutions that can be made to improve the project's environmental consequences.

During the development of this project the main activity required the use of the laptop (programming, simulating and writing) and the room lighting during the hours at the laptop. On the other hand, the laptop kept working on the CFD out of working hours. The total energy is shown on the next table.

Activity	Hours	Energy consumption (kW)	Total energy consumption (kWh)
Laptop	600	0.065	39
CFD simulations	105	0.065	6.83
Lighting	600	0.028	16.8
Total			62.63

Table 6.1: Electrical consumption.

The Catalan Autonomic Government states that the Spanish CO_2 emission in 2022 is 259 gCO_{2eq}/kWh [4]. Based on this value, this project's generates **16.22 kg** of CO_2. On the other hand, as nuclear waste is a great concern for the environment, the generated nuclear waste is stated to be 0.01065 m^3/GWh [24], therefore the project generates **0.00067** m^3 of nuclear waste.

Although nuclear energy seems a worrying subject, it is clear that the amount CO_2 of emissions are far lower than that of a thermal central. A switch to nuclear energy source that supports renewable energy options could reduce the environmental stress that generates human activities.

7 Conclusions

On this study an initial model has been calculated. This required defining the general aircraft arrangement, selecting wing and empennage airfoil data and gathering a boat-plane hull physical model. The obtained results were useful to define the base TO performance of the amphibian aircraft.

The hydrofoil design begun by selecting the desired lift coefficient, which defined the A_1 value. This is the only unknown variable of the J3T and J5T solution. As a result, the foil intrados was calculated. For the case of the hydrofoil extrados, no solver is established. As a consequence, various designs were simulated in OpenFOAM where one was selected.

Comparing the obtained force coefficients of the hydrofoil with previous studies, the results appeared reasonable. Hence, the hydrowing design process was carried out. During the development, it became difficult to obtain an acceptable configuration that could indeed improve the TO performance. On the only case where improvement was attainable, it presented important structural flaws because of the small size of the hydrowing.

Although the design outcome was non viable, an economic feasibility study was carried out. The reason was that a improved hydrofoil design may be viable and therefore, its economic feasibility can be relevant. The study proved the business viability of the project.

After carrying out the preliminary study of a hydrofoil for amphibian aircraft, it has been concluded the non viability of the design. The hydrofoil has no problem on generating enough lift force to elevate the whole aircraft by itself. However, the greatest drawback is the substantial drag generation. The main reason behind this phenomenon appears to be the selected J3T solution. Maybe for a lower C_l the hydrofoil could still lift the aircraft without generating that much drag as the generated intrados geometry would be flatter.

On the other hand, the relatively high TO speed can be the main reason behind the unsuccessful result. It can not be forgotten that the Lisa Akoya is on the market, a light weight aircraft with low TO speed. In addition, racing sail boats do not exceed the $28 m/s$ mark either. As a consequence there is not a large amount of data for this higher flow regimes.

As the project's business model seems viable, the motivation to study different approaches for this preliminary design rises. The proposed idea for further investigation is to select a J3T or J5T solution for a $C_{l_h} = 0.25$ or lower. If none of these hydrofoils substantially reduce the TO run, the preliminary study should be seen as non attainable.

8 Bibliography

[1] Imad Shakir Abbooda et al. *Properties evaluation of fiber reinforced polymers and their constituent materials used in structures – A review*. 2020. URL: https://www.sciencedirect.com/science/article/pii/S2214785320357618.

[2] Stefano Brizzolara. *A New Family of Dual-Mode Super-Cavitating Hydrofoils*. Report. MIT, 2015.

[3] Luis Calvo. *Canadair CL-215T/415*. URL: https://fly-news.es/especial-75o-aniversario-aga/canadair-cl-215t-415/.

[4] Generalitat Catalana. *Factor de emisión de la energía eléctrica: el mix eléctrico*. 2022. URL: https://canviclimatic.gencat.cat/es/actua/factors_demissio_associats_a_lenergia/.

[5] Sinchai Chinvorarat. *Takeff Performance of a Light Amphibious Airplane*. Report. King Mongkut's University of Technology North Bangkok, 2020.

[6] Carlos Cuesta Simón. "Study of the Active Flow Control of an Airfoil". Bachelor's Thesis. UPC, 2019.

[7] America's Cup. *Prada Cup Semi-Final Day 1*. URL: https://www.americascup.com/en/news/1019_PRADA-CUP-SEMI-FINAL-DAY-1.

[8] Projects Department. *Aerospace Engineering Projects. S08. Cost Estimation*. 2020.

[9] Icon. *Discover adventure flying*. 2011. URL: https://www.iconaircraft.com/a5/.

[10] Virgil E. Jr. Johnson. *THEORETICAL AND EXPERIMENTAL INVESTIGATION OF SUPERCAVITATING HYDROFOILS OPERATING NEAR THE FREE WATER SURFACE*. Technical Report. NASA, 1961.

[11] Lisa. *Lisa Akoya, a new generation of seaplanes*. 2011. URL: http://lisa-airplanes.com/en/light-amphibious-aircraft-akoya/performance-and-versatility/landing-on-water/.

[12] Enrique Ortega. *Finite Wing*. 2020.

[13] David Quam. *Mallard on a Hydrofoil*. 2008. URL: https://youtu.be/yolgS1bn7P8.

[14] Salazar S. *Características Mecánicas del Acero*. 2012. URL: https://ingemecanica.com/tutorialsemanal/tutorialn100.html.

[15] Salazar S. *Propiedades Mecánico-Químicas del Aluminio*. 2012. URL: https://ingemecanica.com/tutorialsemanal/tutorialn110.html.

[16] Mohammad H. Sadraey. *Aircraft Design. A Systems Engineering Approach*. 2012.

[17] Seamax. *Seamax aircraft*. 2011. URL: https://www.seamaxaircraft.com/.

[18] Arjit Seth and Rhea P. Liem. *Takeoff analysis of amphibious aircraft with implementation of a hydrofoil*. Paper. 2018 Structures Congress, 2018.

[19] Shinmaywa. *Performance of the State-of-the-Art US-2*. URL: https://www.shinmaywa.co.jp/aircraft/english/us2/us2_capability.html.

[20] Henry B. Suydam. *HYDRODYNAMIC CHARACTERISTICS OF A LOW-DRAG, PLANING -TAIL FLYING-BOAT HULL*. Technical Note. NACA, 1952.

[21] Teknika4. *Aluminio Aeronáutico*. 2009. URL: https://www.teknika4.com/es/aluminio-aeronautico.

[22] Nicholas J. Vagianos, David B. Thurston, and Thurston Aircraft Corporation. *Hydrofoil Seaplane Institution*. Report. US NAVY, 1970.

[23] Viking. *Twin Otter Seres 400*. 2010.

[24] WWF. *Observatorio de la Electricidad*. 2022. URL: http://awsassets.wwf.es/downloads/observatorio_electricidad_wwf_noviembre_09.pdf.